# Test Report

# Ocean Testing of the Prototype Azura Wave Energy Converter June 2015 – March 2016

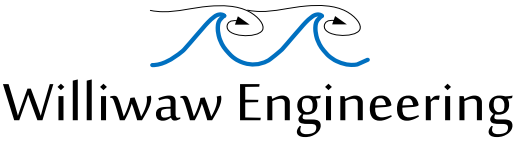


Prepared for

Hawaii National Marine Renewable Energy Center (HINMREC)
Hawaii Natural Energy Institute (HNEI)
University of Hawaii

April 2016

This document was prepared following HINMREC/HNEI specifications and review. This work was funded by the US Department of Energy's Wind and Water Power Program under Award DE-FG36-08GO18180 to HINMREC/HNEI of the University of Hawaii

# Revisions

Revisions

| Revision # | Date | Revised By | Description |
|---|---|---|---|
| Revision 0 | 4/13/2016 | Terry Lettenmaier | Initial Draft |
| Revision 1 | 4/20/2016 | Terry Lettenmaier | Revise per UH comments |
| | | | |
| | | | |
| | | | |

# Table of Contents



# Table of Appendices

# 1. Introduction

This document describes ocean testing of the Northwest Energy Innovations (NWEI) prototype Azura wave energy converter at the Naval Facilities Engineering Command (NAVFAC) 30-meter Wave Energy Test Site (WETS 30m Site) in Hawai'i. The WETS 30m site is located at the Kaneohe Marine Corps Base Hawai'i (MCBH) on the northeast coast of the island of O'ahu. The Azura prototype test has been a cooperative effort of NWEI, NAVFAC, University of Hawaii's Hawaii National Marine Renewable Energy Center (HINMREC), and the U.S. Department of Energy's National Renewable Energy Laboratory (NREL). The Azura was deployed on May 27-30, 2015 for a one year period. This report describes the results of this testing through March 2016.

# 2. Test Plan and other Reference Documents

The following documents are referenced elsewhere in this report.

## 2.1 Test Plan

The NWEI document *Test Plan - NWEI Wave Energy Demonstration at the Navy's WETS 30m Project Site* includes a description of the test article, test objectives, test setup, and test instrumentation.

## 2.2 Other Reference Documents

The following documents describe aspects of the prototype Azura deployment not covered in this report, including preliminary testing of the device power take-off (PTO) that was performed prior to the WETS deployment and the grid interconnection system used to connect the device at WETS:

- *Dry Testing of the Azura PowerPod at Energy Hydraulics Ltd* (Williwaw Engineering test report) describes PTO testing performed prior the WETS deployment at the facilities of Energy Hydraulics Ltd. in New Zealand where the PTO was built.
- *Interconnection of a 20kW Wave Energy Device at the WETS 30m Site* describes details of the grid interconnection system used for the prototype Azura at the 30m WETS site.
- *Low Power Testing of Grid Interconnection System* (NWEI test report) describes testing of the prototype Azura grid interconnection system prior to Azura deployment.
- *Grid Interconnection Performance Assessment and Final Report* (NWEI report) provides an assessment of the Azura grid interconnection system after the Azura deployment.
- *After Action Report: AB Mooring Modification* (NWEI report) describes the modifications to the Azura prototype mooring system that were made on January 8, 2016.
- IEC Technical Specification 62600-100, *Marine energy – Wave, tidal and other water current converters – Part 100: Electricity producing wave energy converters – Power performance assessment* describes methods to assess power performance of WECs.

# 3. Timeline

Table 3-1 shows the major events that occurred during the prototype Azura deployment from late May 2015 through March 2016. A corresponding timeline of device configurations together with device control methods during the same period are shown in Figure 3-1.

When the device was deployed in late May 2015, the mooring system was not installed as designed because the lengths of the mooring lines were incorrect for the fixed anchor locations. These anchor locations were existing from a previous project and were not located where expected. As a result, the "subsurface" float on the south or AB mooring leg was not pulled below the surface. This caused lower than expected mooring pre-tensions and high wave forces on this float and the AB mooring leg, which ultimately caused the attachment of this float to fail and this float to break free in mid-November 2015. In early January 2016, the AB subsurface float was re-installed and modified mooring lines were installed to make the mooring system consistent with the original design. Because the 2015 mooring configuration did affect device performance to some extent, data collected after the January 2016 mooring modification has been used for this report whenever possible. Refer to the NWEI report *After Action Report: AB Mooring Modification* for further details regarding this mooring system modification.

In late November 2015, a hydraulic oil hose connection to one of the main cylinders on board the prototype Azura came loose and the leaked hydraulic fluid. The device was not operational for a 12 day period until this connection was tightened and hydraulic fluid re-filled. The device was operational for the remainder of the June 2015 through March 2016 period.

**Table 3-1 Major events during Azura prototype testing**

| Test | Date |
|---|---|
| Installation of prototype Azura at 30m WETS site | May 27-30, 2015 |
| Device connected to grid and produces power for first time | June 1, 2015 |
| Hawaiian Electric Company (HECO) gives permission to operate | June 29, 2015 |
| Mooring subsurface AB float breaks loose | Nov. 16, 2015 |
| Device stops producing power due to loss of PTO hydraulic fluid | Nov. 26, 2015 |
| Device operation resumes; PTO hose tightened and re-filled with hydraulic fluid | Dec. 7, 2015 |
| K-Bay Waverider buoy mooring failure – data recording stops | Dec. 21, 2015 |
| Moorings repaired: AB float re-installed and AB mooring riser shortened to put AB float at proper depth below surface | Jan. 8, 2015 |
| K-Bay Waverider buoy re-deployed – data resumes | Jan. 14, 2015 |

Figure 3-1 shows the device configurations and control methods in place from June 2015 through March 2016. The hydraulic PTO of the prototype Azura can be operated with two different control methods: 1) constant settings of hydraulic motor displacement, and 2) proportional-integral (PI)

control of the hydraulic motor displacement. See the test report *Dry Testing of the Azura PowerPod at Energy Hydraulics Ltd* for a detailed description of these two control methods. The constant displacement motor control is a simple control method that is easier to implement in computer models of the Azura PTO system than the PI control. Because the use of prototype Azura data to validate computer models of the device has been a high priority, large periods of the prototype Azura deployment have been dedicated to collecting data while the device has been operated with different constant hydraulic motor displacement settings. During these time periods, six alternate settings of hydraulic motor displacement have been used, with the setting automatically changed between the alternate settings every 30 minutes on the even half hour. Because PI control has potential to increase device output power relative to constant displacement control, experimentation with different PI control settings was also performed during other time periods.

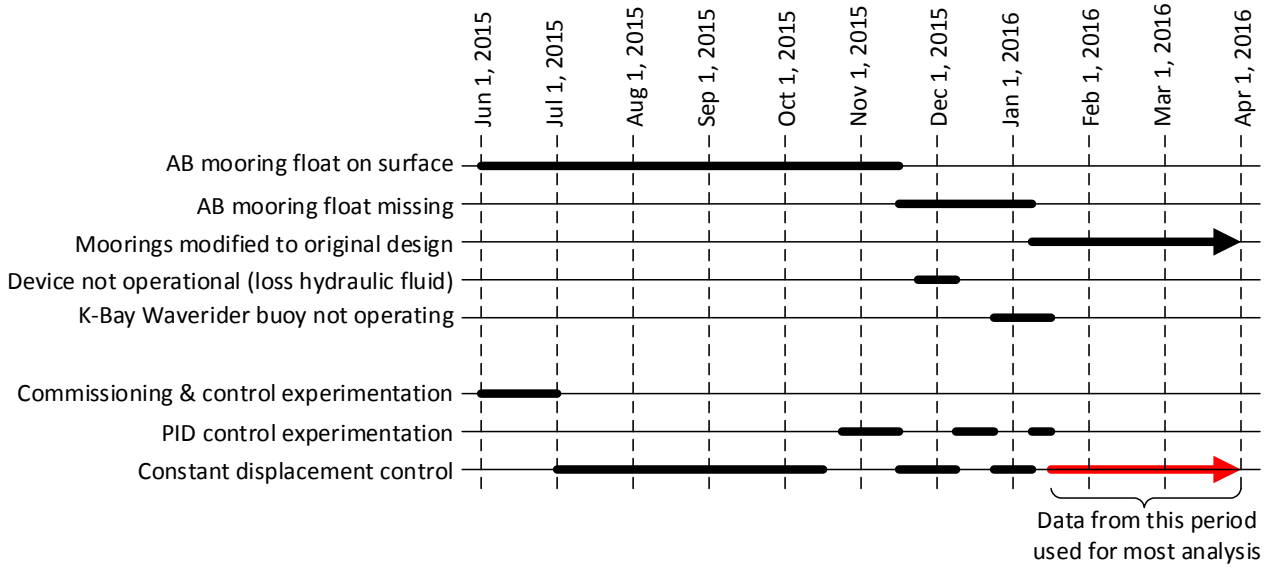


**Figure 3-1 Timeline of device configurations and control modes during prototype Azura testing**

## 4. Test Setup

The test setup for Azura prototype testing is described, in detail, in the test plan and also the grid interconnection report referenced in Section 2.

# 5. Test Results

The test results presented in this report primarily focus on measurements of device power performance and operating characteristics made during January through March 2016 after the mooring system was modified. This data was used to eliminate effects of the 2015 mooring installation where one of the "subsurface" mooring floats was on the surface, as described in Section 3. Almost all operation during this time period was with the PTO control in constant hydraulic motor displacement mode. This control method is of most interest for validation of computer models for the prototype Azura design. Sea conditions and availability data for June 2015 through March 2016 are presented, however, to provide information related to device survivability for the entire deployment period.

## 5.1 Sea conditions June 2015 – March 2016

The distribution of significant wave heights ($H_{m0}$) and energy periods ($T_e$) that the prototype Azura operated in from June 2015 through March 2016 are shown in Figure 3-1, based on data recorded by the Kaneohe Bay Waverider Buoy that is deployed at the WETS 80 m site, which is about one mile northwest of the WETS 30 m site where the prototype Azura is deployed. Spectral data recorded by this buoy was corrected for shoaling using linear wave theory to the 30 m depth of the WETS 30m site. The $H_{m0}$ and $T_e$ data used for Figure 3-1 were calculated from the 30 m corrected spectral data. The sample counts shown in Figure 3-1 are the number of 30 minute data samples when the Azura was operating (producing power to the grid) for at least 20 minutes.

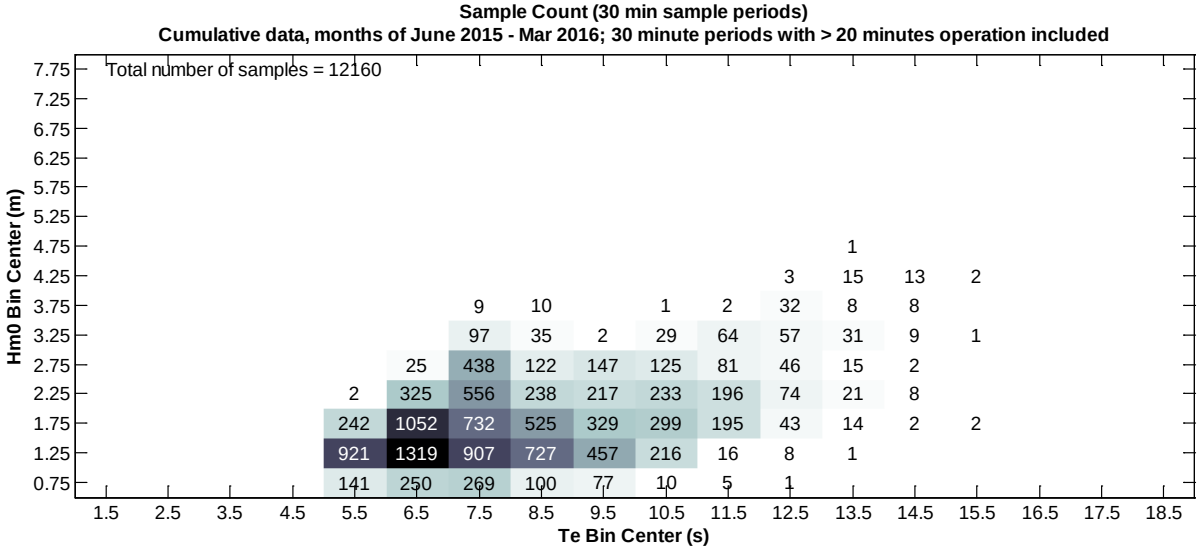


**Figure 5-1 30 minute sample count June 2015 – March 2016**

The maximum wave heights that occurred during the June 2015 – March 2016 period are shown in Table 5-1. The maximum wave heights were determined by analyzing time series water surface elevation data recorded by the Waverider buoy at the WETS 80m site. The largest $H_{m0}$ for a half hour period was 4.5 m, while the largest single wave height was 7.5 m.

**Table 5-1 Maximum wave heights at WETS 80m site June 2015 – March 2016**

| Date and time (UTC) (half-hour period) | Hm0 (m) | Te (s) | Maximum wave height (m) |
|---|---|---|---|
| 2-23-2016 8:00 | 4.5 | 13.6 | 7.2 |
| 2-23-2016 11:00 | 4.5 | 13.2 | 6.3 |
| 2-22-2016 18:00 | 4.4 | 15.0 | 6.2 |
| 2-23-2016 1:30 | 4.4 | 14.7 | 6.4 |
| 2-23-2016 1:00 | 4.4 | 14.7 | 6.7 |
| 2-23-2016 4:00 | 4.4 | 13.7 | 7.5 |
| 2-23-2016 9:30 | 4.3 | 13.4 | 6.5 |
| 2-23-2016 5:30 | 4.3 | 13.4 | 6.3 |
| 2-23-2016 10:00 | 4.3 | 13.1 | 6.5 |
| 2-22-2016 17:30 | 4.3 | 14.4 | 5.1 |

## 5.2 Device availability June 2015 – March 2016

The percent availability of the Azura prototype by month is shown in Figure 5-2. Availability was calculated as the ratio of the number of device operating minutes (when the device was producing power to the grid) to the number of minutes in each month. The major non-operational periods are listed in Table 5-2. The only period when the device was not capable of operating during the months of June 2015 through March 2016 was the 12 day period in late November and early December 2015 after PTO hydraulic fluid was lost due to a loose hose connection. Numerous other short non-operating periods occurred throughout the deployment, however, usually for one of the following reasons:

- Device shut downs after faults were detected by the controller. Most often, faults were caused by momentary losses of grid voltage on shore. Some faults were also caused by controller software errors. In all cases, the faults needed to be investigated then manually reset before device operation resumed.
- Intentional non-operating periods while no-load device data was collected.
- Shut downs during at-sea maintenance of the device.

The non-operational time of the prototype Azura could be reduced by implementing automatic reset of the controller after faults occur. While this would be a normal controller function in a production device, it was not considered necessary for this prototype test.

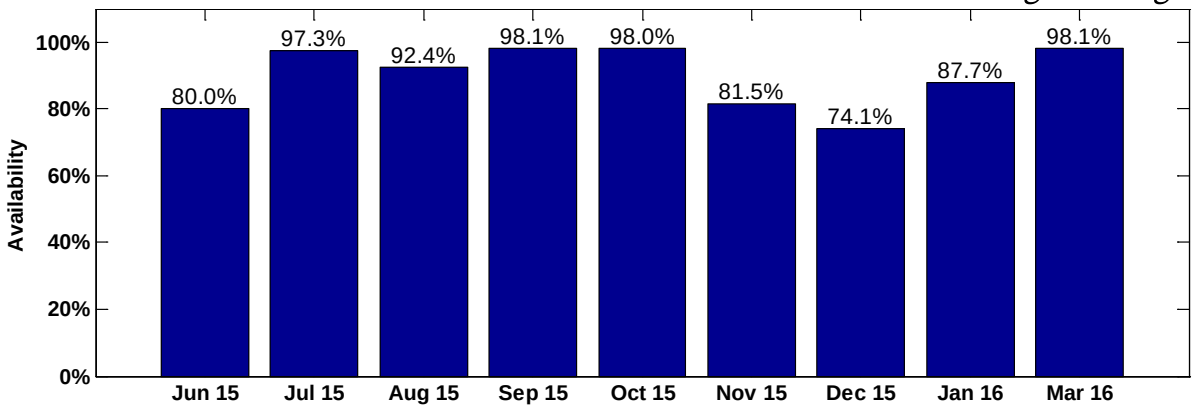


**Figure 5-2 Prototype Azura availability by month June 2015 – March 2016**

**Table 5-2 Major prototype Azura non-operational periods June 2015-March 2016**

| Month | Major non-operating periods |
|---|---|
| June 2015 | Numerous shut downs because device not continuously operated prior to Hawaiian Electric permission to operate on June 29, 2015 |
| Nov & Dec 2015 | No operation for 12 days due to hydraulic oil loss caused by loose hose connection. |
| Jan 2016 | Two day shut down during mooring work. |

## 5.3 Power Performance per IEC 62600-100 Technical Specification

Power performance of the prototype Azura was assessed per the IEC Technical Specification 62600-100 described in Section 2.2. Results are presented in Figure 5-3 through Figure 5-8 for January – March 2016 while the device was operated with constant hydraulic motor displacement control of the PTO. During most of this time period the control setting was automatically changed between the six different hydraulic motor displacement settings 30, 35, 45, 55, 65, and 80 cc/rev every 30 minutes at each even half-hour. Using this method equal test time was dedicated to each motor displacement control setting. The number of 30 minute data samples used for this assessment are shown in Figure 5-1.

Because the prototype Azura test setup uses low voltage dc transmission through the subsea cable to shore, dc electrical power $P_{dc}$ measured at the output terminals of the device was used for this assessment rather than 60 Hz ac output power as specified in IEC 62600-100 Section 8.1. See the NWEI document *Interconnection of a 20kW Wave Energy Device at the WETS 30m Site* for details regarding the prototype Azura grid connection. The $P_{dc}$ measurement was verified to have an accuracy of 2% or better during dry tests of the Azura PowerPod performed prior to deployment.

Per IEC 62600-100, normalized power (Figure 5-4) was calculated from mean capture length (Figure 5-5) and the energy flux of representative spectra for each $H_{m0}$-$T_e$ bin. Capture length (m) is the ratio of mean device output power (W) to wave energy flux (W/m) for each thirty minute period. The wave energy flux for each 30 minute period was calculated from thirty minute wave spectra data recorded by the Kaneohe Bay Waverider buoy that is deployed at

the WETS 80m site. This is a Datawell DL Waverider buoy that has been deployed by the University of Hawaii. The wave spectra were corrected for shoaling to 30m depth using linear wave theory, then the corrected spectra were used to calculate wave energy flux. The representative spectra used to calculate normalized power in each bin per IEC 62600-100 is the average of all 30 m corrected spectra recorded for each bin, shifted in magnitude and frequency so that the $H_{m0}$ and $T_e$ of the average spectra are at the center of each bin.

The standard deviation of capture length, maximum capture length, and minimum capture length are also shown in Figure 5-6, Figure 5-7, and Figure 5-8, respectively, per IEC 62600-100.

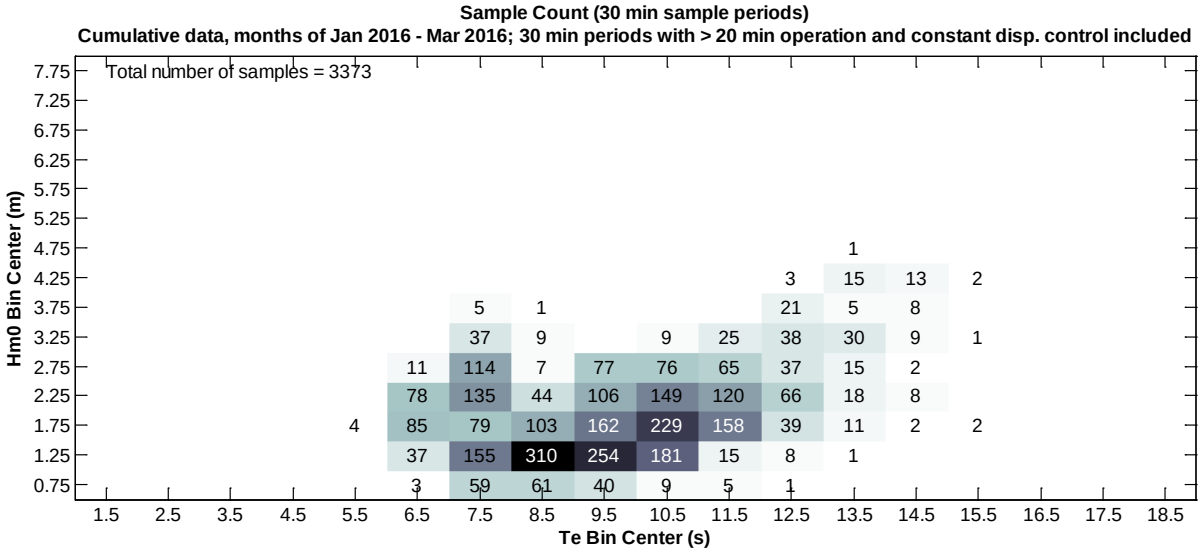


**Figure 5-3 30 minute sample counts**

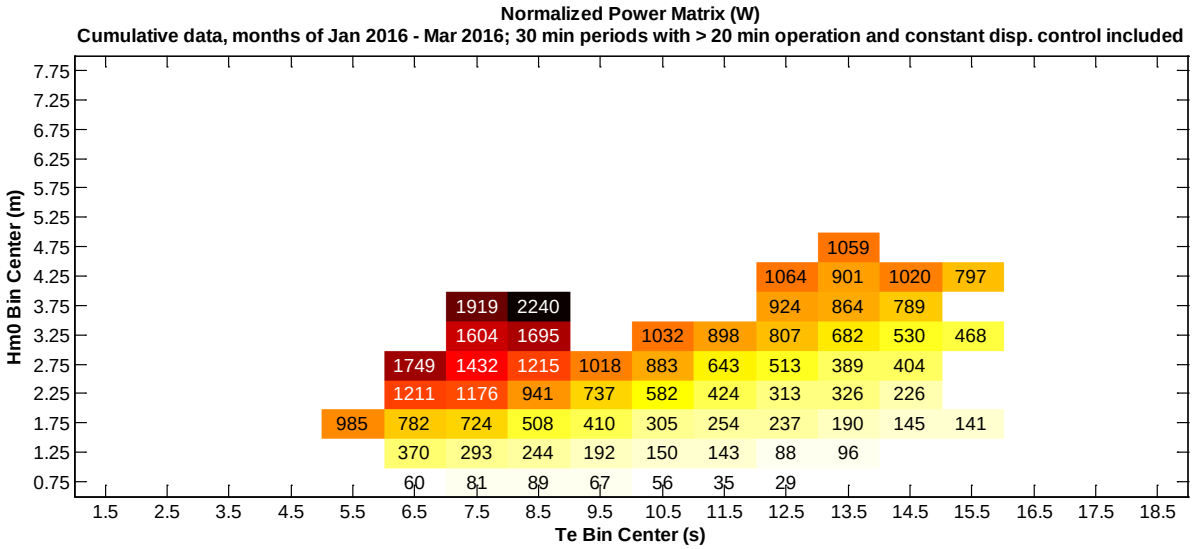


**Figure 5-4 Normalized power matrix**

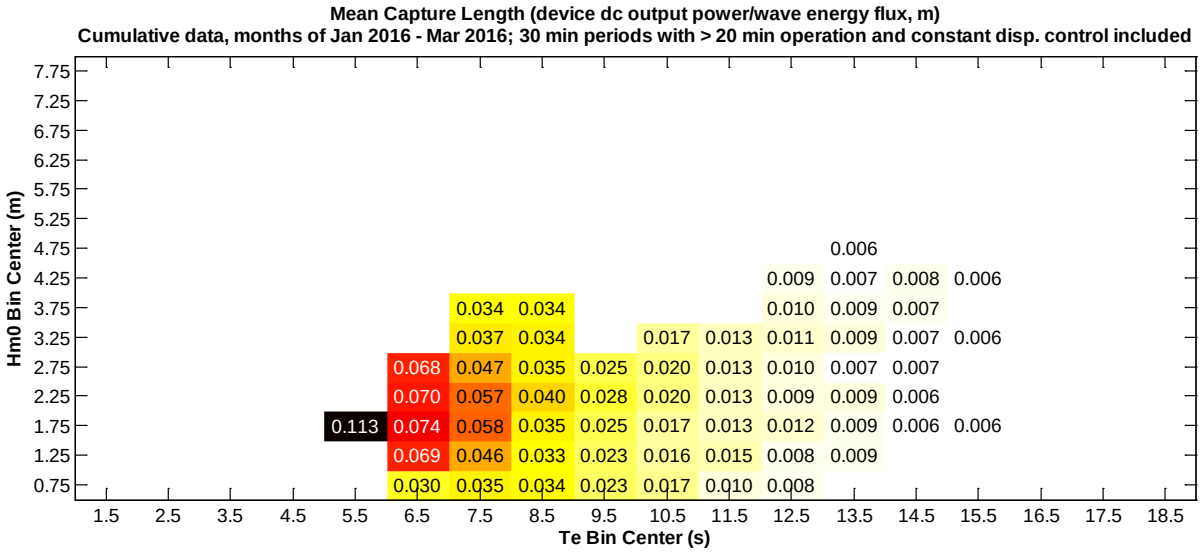


**Figure 5-5 Mean capture length**

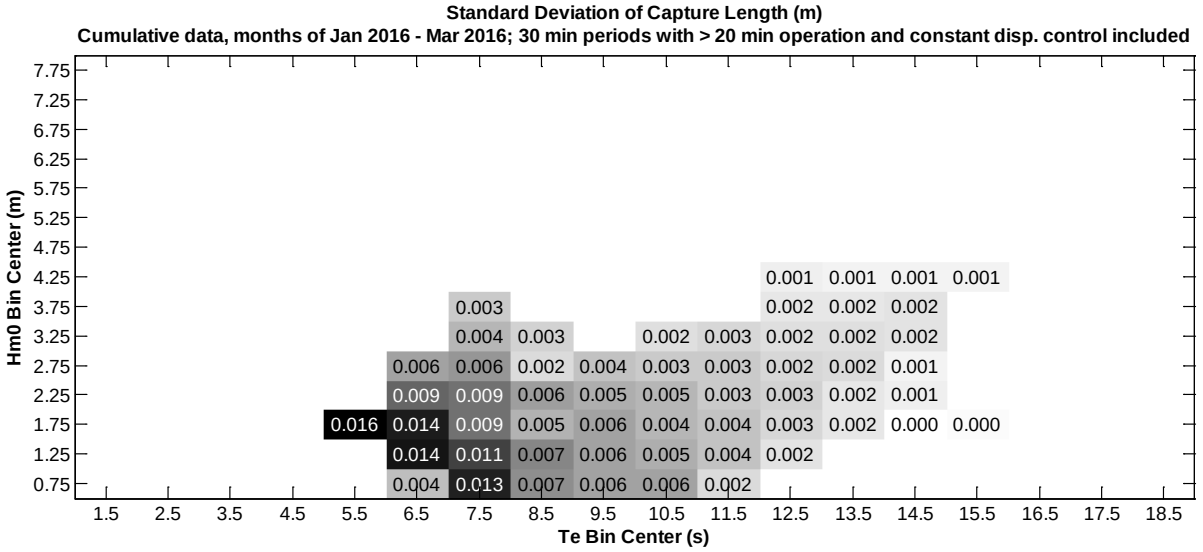


**Figure 5-6 Standard deviation of capture length**

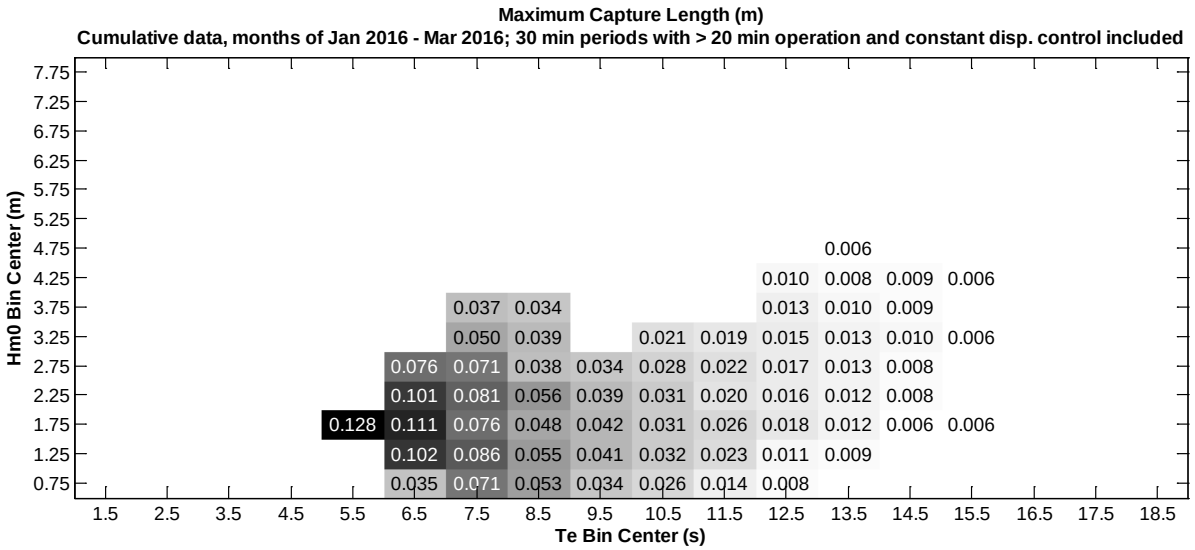


**Figure 5-7 Maximum capture length**

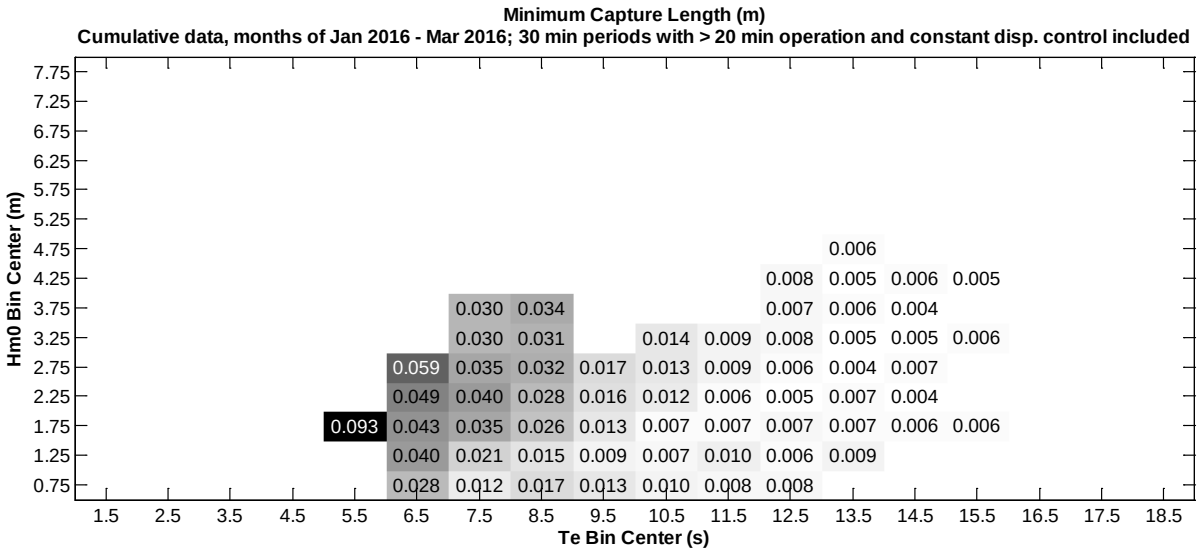


**Figure 5-8 Minimum capture length**

## 5.4 Other power performance measurements

The normalized power matrix shown in Figure 5-4, in accordance with IEC 62600-100, includes a correction to device power measurements when average wave conditions are not in the center of each $H_{m0}$ and $T_e$ bin. The correction factor applied to each bin is approximately $H_{m0\_center}^2/H_{m0\_avg}^2 * T_{e\_center}/T_{e\_avg}$ where average $H_{m0}$ and $T_e$ values are calculated from moments of the average of all wave spectra recorded in each bin and the center $H_{m0}$ and $T_e$ values are the bin centers. The uncorrected mean power matrix of data recorded during the same time period, which is not required by IEC 62600-100, is shown in Figure 5-9. This matrix simply shows the average of all 30 minute output power measurements made in each bin. The percent differences, bin by bin, between the normalized power matrix (Figure 5-4) and the

mean power matrix (Figure 5-9) are shown in Figure 5-10. These differences can be substantial when the average $T_e$ and/or $H_{m0}$ in a particular bin differs substantially from the bin center.

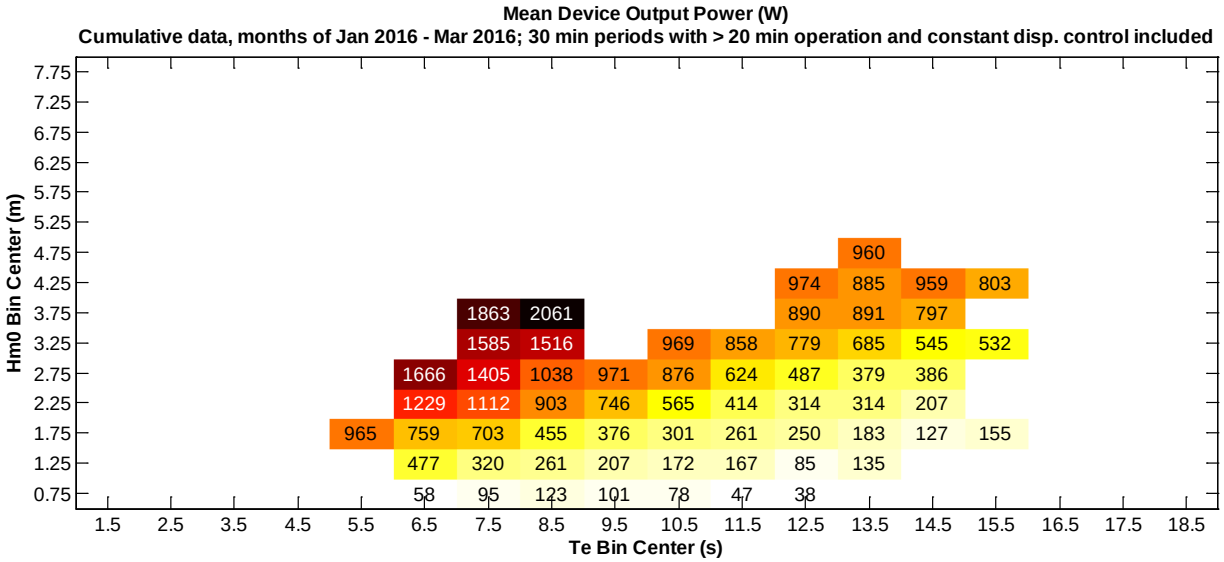


**Figure 5-9 Mean power matrix**

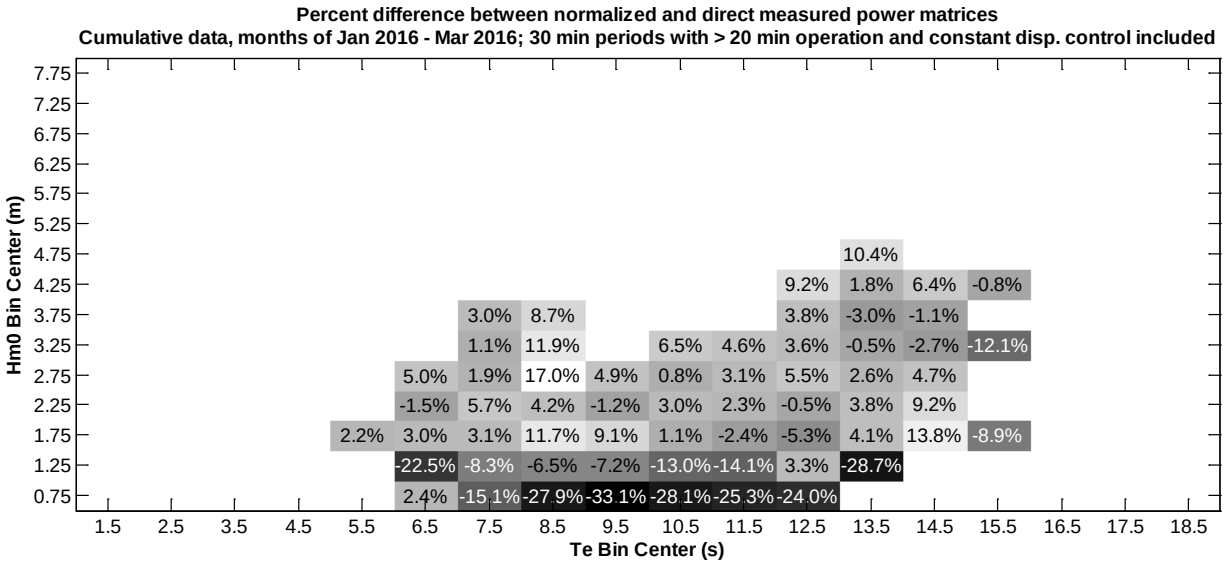


**Figure 5-10 Percent difference between normalized power (Figure 5-4) and mean power (Figure 5-9)**

A matrix of 95th percentile power measurements for the January – March 2016 period is shown in Figure 5-11. This shows the 95th percentiles of all the uncorrected 30 minute output power measurements that were made in each bin. During this time period the device PTO was operated alternately with six different hydraulic motor displacement settings. The hydraulic motor displacement setting affects device output power to some extent (see Section 5.5). One way that power performance of the device could be improved is to always adjust the motor displacement to the optimum setting for the wave conditions that exist. While there are no

plans to test this method during the prototype Azura deployment, the 95th percentile power matrix shown in Figure 5-11 shows the potential output power that may be possible in each bin with an ideal motor displacement setting. Results are not included in Figure 5-11 for bins that have less than three data samples, to avoid low 95th percentile results that may occur when sample size is extremely small.

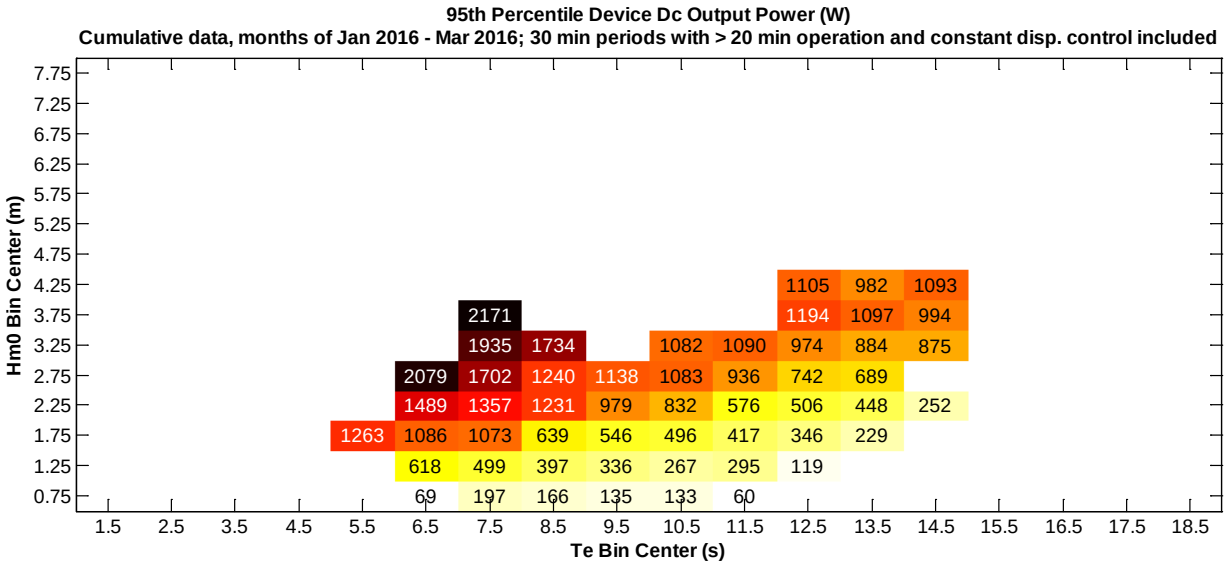


**Figure 5-11 95th percentile power matrix**

## 5.5 Effect of PTO hydraulic motor displacement on output power

Thirty minute average output power for the prototype Azura is plotted against PTO hydraulic motor displacement setting in Figure 5-12. PTO input power, calculated from the product of hydraulic pressure and hydraulic flow, is also shown (in blue) in Figure 5-12. Data from the same January through March 2016 period used for the power performance assessments in Sections 5.3 and 5.4 were used for these plots. The plots are binned by $H_{m0}$ and $T_e$ in the same way as the power performance data. Only bins with larger $H_{m0}$ and smaller $T_e$ are plotted; these are the conditions where the device produces the most power. The motor displacement setting in the PTO changes the average damping, or the amount of force applied to the device float relative to the rotational velocity of the float. Decreasing motor displacement increases average damping, so that the average damping applied to the float is highest at the minimum motor displacement of 30 cc/rev.

In general, Figure 5-12 shows relatively small variations in output power with respect to motor displacement in each bin. A significant trend in both output power and PTO input power can be seen with respect to motor displacement, however, in the 3.25m $H_{m0}$ and 7.5s $T_e$ bin. This is the highest $H_{m0}$ bin that has enough data to plot and this result may indicate that in larger, short period waves the device benefits from higher damping of the float. Other output power variations that are independent of motor displacement could be caused by differences in wave spectral shapes for different 30 minute data samples collected in the same bin.

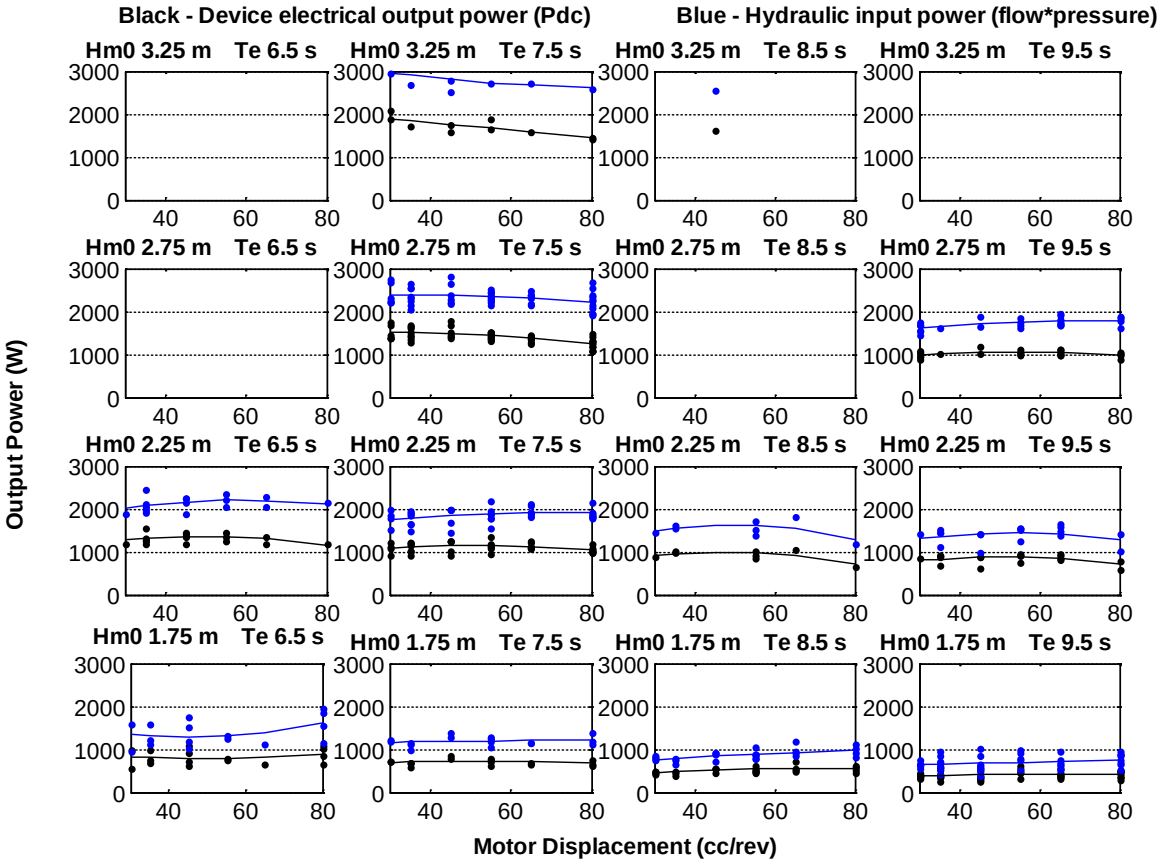


**Figure 5-12 Device power versus motor displacement setting January-March 2016**

## 5.6 Effect of proportional-integral control on output power

The prototype Azura was tested with proportional-integral (PI) control of PTO hydraulic motor displacement during different periods of time during October 2015 through January 2016 (see Figure 3-1 timeline). During the remainder of testing, constant hydraulic motor displacement settings were used. See the test report *Dry Testing of the Azura PowerPod at Energy Hydraulics Ltd* for a detailed description of both the PI and constant displacement methods of controlling the Azura PTO. Constant displacement motor operation is a simple method that is easier to implement in computer models. PI control is used to automatically adjust motor displacement in order to keep hydraulic cylinder pressure proportional to hydraulic flow. This has potential to improve performance of the prototype Azura because cylinder pressure is proportional to the force applied to the float while cylinder flow is proportional to the velocity of the float. When pressure is kept proportional to flow, constant damping results with float force proportional to velocity, which is expected to improve hydrodynamic performance when the force to velocity ratio or damping is adjusted to an optimum value. The effectiveness of the PI control in the prototype Azura is limited, however, by long charge and discharge times of the PTO accumulator that make effective PI pressure regulation challenging.

Experimentation with numerous parameter settings of the PI algorithm were carried out during the October 2015 through January 2016 testing including 1) damping constant, 2) minimum pressure command, 3) and flow averaging time. Due to limited test time a complete

assessment of the effectiveness of PI control with different combinations of these parameter settings was not possible across a wide range of sea conditions. Also, much of this PI control testing was performed while the AB subsurface mooring float was missing (see Figure 3-1 timeline). Since the loss of the AB float may have affected power performance results, this makes direct comparison to constant motor displacement results during other time periods more difficult. A very rough comparison can be made between power performance with PI control and constant displacement control by simply comparing 95$^{th}$ percentile results. This compares the best output power that was achieved with different settings of the PI control to the best achieved with constant displacement.

The number of thirty minute sample counts accumulated while operating with PI control during October 2015 through January 2016 are shown in Figure 5-13. This represents 625 hours of operation. The corresponding 95$^{th}$ percentile power matrix is in Figure 5-14, which gives an indication of the best 30 minute average power that was achieved with PI control. Results are only included for bins that have at least three samples to avoid low 95th percentile results that may occur when sample size is extremely small. These numbers give an indication of how well the PI control did with the best settings that were tested. In Figure 5-15, a percent comparison is shown between the Figure 5-14, 95$^{th}$ percentile results for PI control and the corresponding Figure 5-11 results for constant displacement control (measured during January through March 2016). Positive percentages in Figure 5-15 indicate that power was higher with PI control than constant displacement control in that bin.

In general, the Figure 5-15 results do not show significant improvements for the PI control relative to constant displacement control in any bins. Because the constant displacement control measurements were made after the January 2016 mooring modifications while the PI control measurements were made before these modifications (see Section 3), this is only a rough comparison. It is unlikely, however, that device output power changed by more than 10% as a result of the mooring changes alone, so the Figure 5-15 results probably indicate that large improvements in output power did not result from using the PI control.

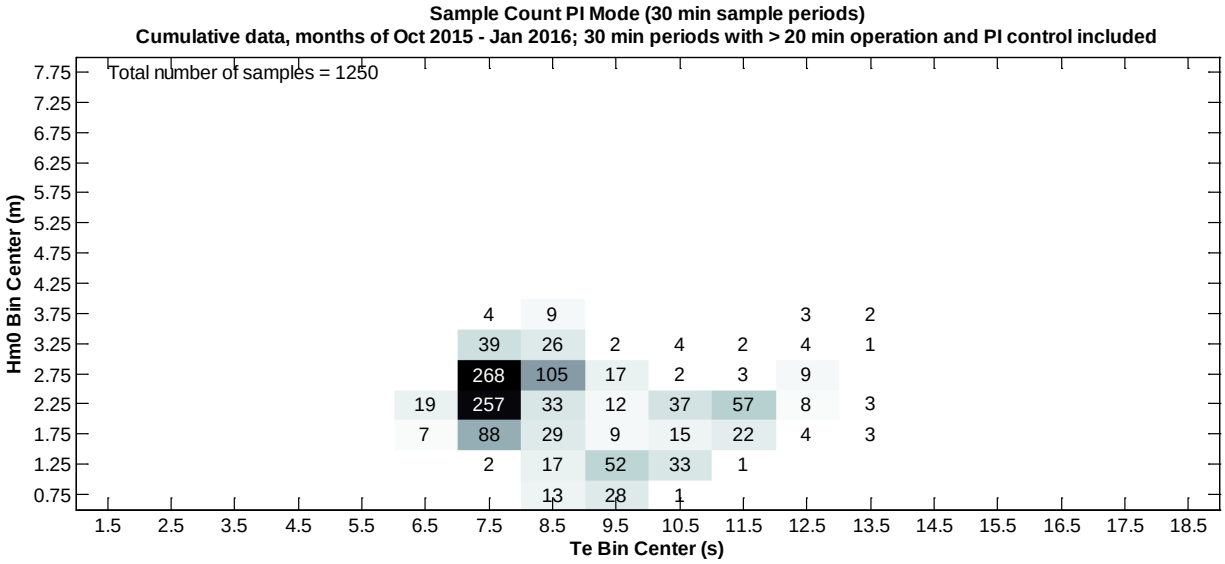


**Figure 5-13 Thirty minute sample count with PI control**

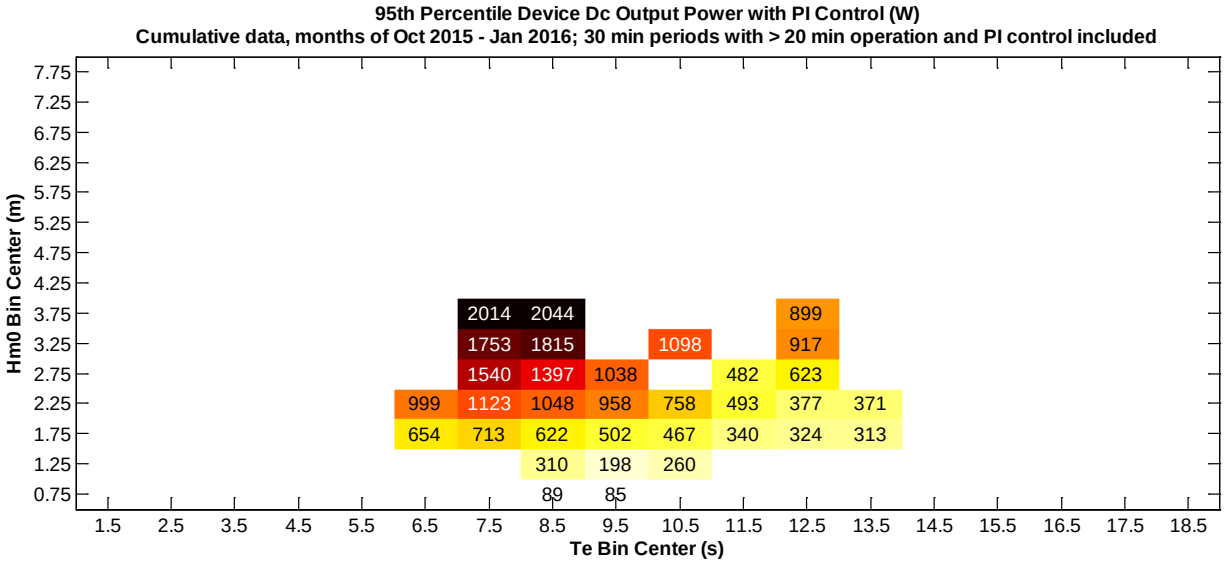


**Figure 5-14 95th percentile power with PI control**

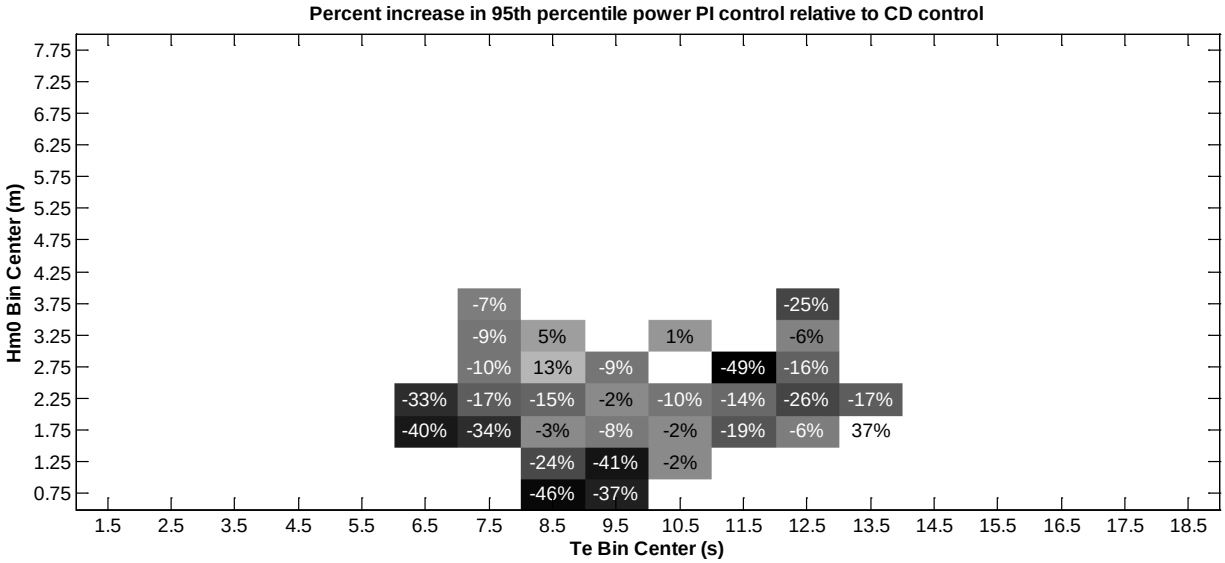


**Figure 5-15 Percent increase in 95th percentile output power with PI control**

## 5.7 PTO Efficiency

Plots of PTO efficiency with respect to device output power are shown in Figure 5-17 for three different motor displacement settings. The same data used for the January through March 2015 power performance assessments described in Section 5.3 were used for this analysis. PTO efficiency was calculated as follows:

$$Efficiency = \frac{P_{out}}{p_{PTO} * Q_{PTO}}$$

Where $P_{out}$ is the electrical output power measured on board the device, $p_{PTO}$ is the hydraulic pressure at the PTO input (PT04-PT03), and $Q_{PTO}$ is the hydraulic flow. See Figure 5-16 for a

diagram of the PTO hydraulics that shows the locations of pressure and flow sensors. This efficiency measurement does not include losses in the hydraulic cylinders or rectifiers. The cylinder and rectifier losses are expected to be small fraction of total PTO losses but sensors were not available to quantify these losses.

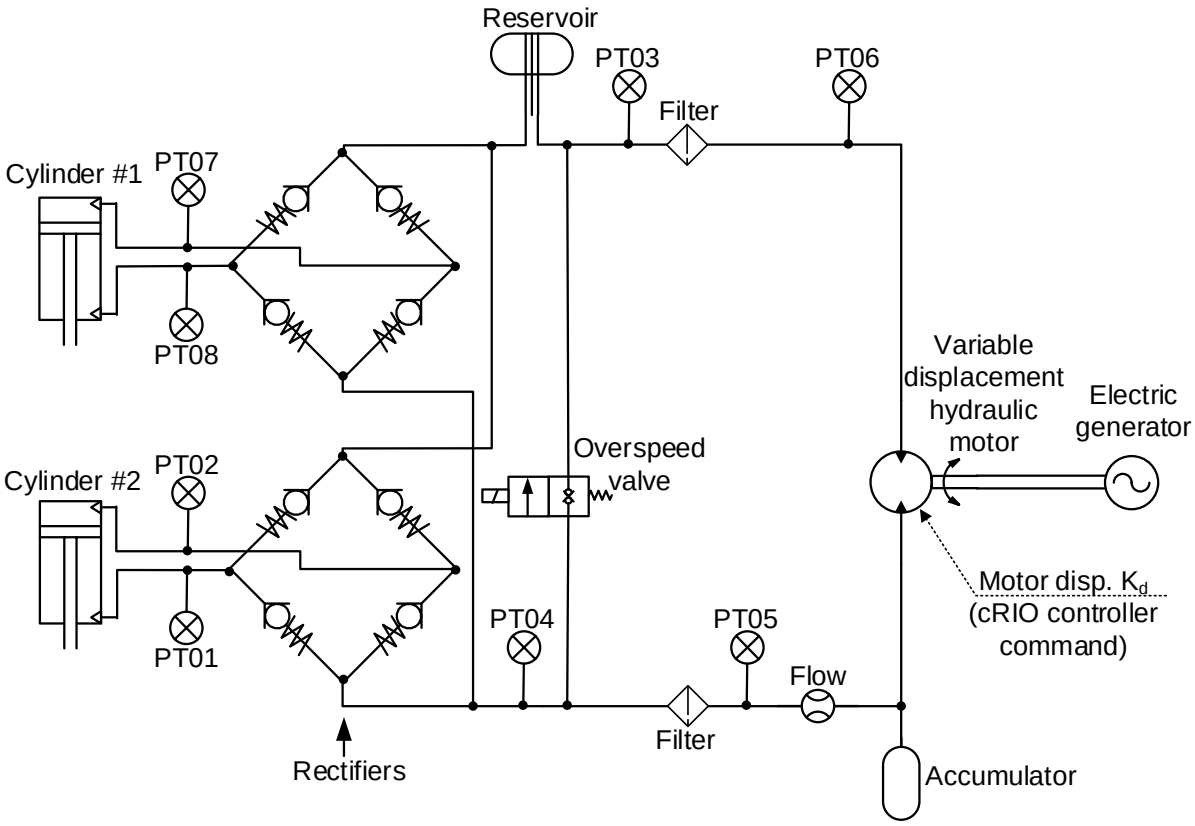


**Figure 5-16 Simplified diagram of prototype Azura PTO hydraulic system**

As shown in Figure 5-17, PTO efficiency was highest when the lowest motor displacement setting of 30 cc/rev was used. This trends was expected. Lower motor displacement generally causes the PTO to operate at higher hydraulic pressure and lower hydraulic flow. Most hydraulic losses are lower at reduced flow. Also, when operating at higher pressure the hydraulic accumulator is more often above its pre-charge pressure. This keeps the hydraulic motor running continuously, smooths output power, and improves motor efficiency.

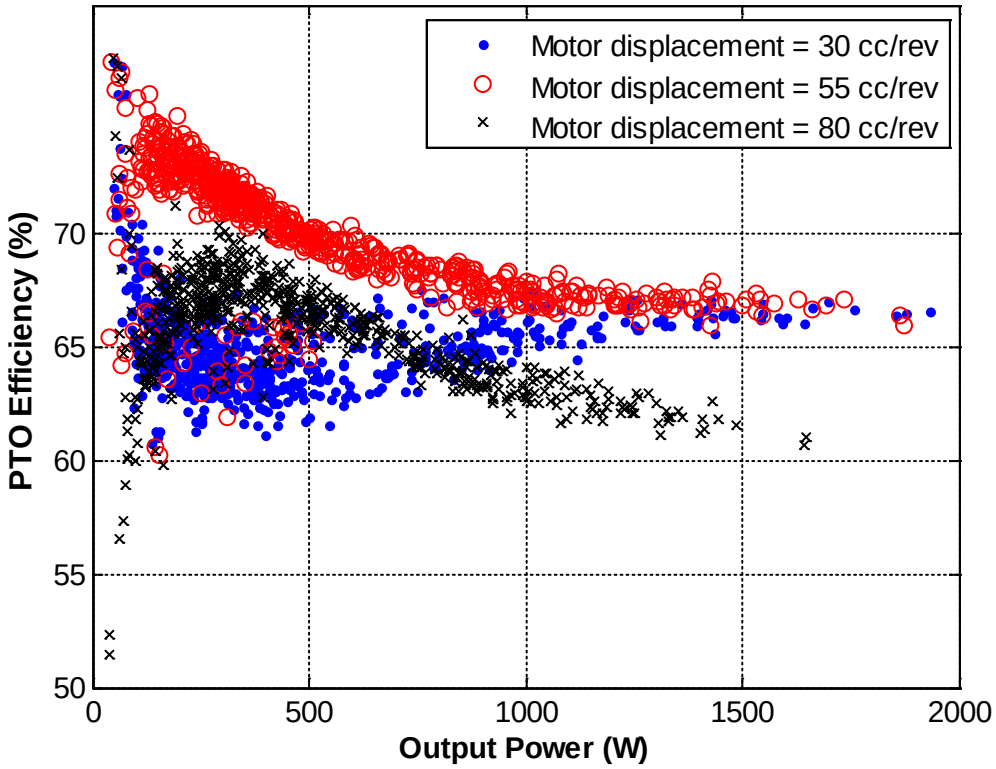


**Figure 5-17 PTO efficiency versus output power**

## 5.8 Device response with respect to wave frequency

Responses of the device with respect to wave frequency (or period) were determined using spectral analysis of time series data recorded on board the device and wave elevation data recorded by the Waverider buoy at the 80m site. Response amplitude operators (RAOs) were calculated to show the motion responses of the device, while relative capture width (RCW) was calculated to show the output power response of the device. In the case of the RAO calculations, in addition to estimating the amplitude responses with respect to Waverider wave measurements, assessments of the device phase responses were also made with respect to wave elevation at the device calculated from hull water pressure sensor data. These RAO and RCW measurements have been especially useful for validating computer simulation models of the prototype Azura.

### 5.8.1 Response Amplitude Operators

Device motion data recorded by an NREL dynamic motion sensor that measures heave displacement, roll, and pitch along with data from an NWEI float angle sensor was used to calculate Response Amplitude Operators (RAOs) for heave, roll, pitch, and float angle. RAOs are transfer functions between the device motion spectra and wave spectra that show the motion response of the device with respect to wave frequency.

Two different methods were used to calculate RAOs from experimental data. The first method used water surface elevation measurements made with the Kaneohe Bay Waverider buoy that is located at the 80 m WETS site. RAO magnitude was calculated using the following equation, where the RAO is defined as the modulus of H(ω):

$$|H(\omega)|^2 = \frac{S_{yy}(\omega)}{S_{xx}(\omega)}$$

Where $S_{xx}(\omega)$ is the wave spectrum measured with the Waverider buoy and $S_{yy}(\omega)$ is the measured response spectrum of device motion measured with either the NREL motion sensor or the NWEI float angle sensor. Fast Fourier transforms (FFTs) of the wave elevation and motion data were used to calculate $S_{xx}(\omega)$ and $S_{yy}(\omega)$, respectively.

The second method used data from a water pressure sensor located on the prototype Azura hull below the water surface to reconstruct water surface elevation data at the device using linear wave theory. Complex RAOs were calculated from this data as follows:

$$H(\omega) = \frac{S_{xy}(\omega)}{S_{xx}(\omega)}$$

Where H(ω) is the complex RAO that includes both magnitude and phase information, $S_{xy}(\omega)$ is the cross-spectrum of wave elevation and device response, and $S_{xx}(\omega)$ is the wave spectrum measured with the Waverider buoy.

The water surface elevation time series at the device was calculated from water pressure and heave data as follows:

$$\eta = \left(\frac{pressure}{\rho g} + heave\right) / \left(\frac{\cosh(k(heave + h + z))}{\cosh(kh)}\right)$$

Where η is the water surface elevation, h is depth (30m), z is nominal pressure sensor depth (6m), heave is the heave displacement measured by the NREL motion sensor, and k is the average value of wavenumber calculated from the 30 minute energy period $T_e$ using linear wave theory.

While wave elevation calculated from the water pressure sensor data is expected to be less accurate than the Waverider data, since it is measured at the device it can be used to calculate valuable RAO phase information that is useful for validating computer model results.

RAO magnitudes calculated using both methods described above and RAO phases calculated using the water pressure data are presented in Figure 5-18 through Figure 5-21, respectively, for hull heave displacement, float angle, hull pitch, and hull roll. These results were generated by calculating RAO results for numerous 30 minute data periods then averaging these together to provide smoothing. The following criteria were used to select the 30 minute data periods that were used for the analysis from all of the January-March 2016 prototype Azura data (all data periods meeting these criteria were used):

- Te<8s and 1.6m<Hm0<2.4m (short period, medium size waves).
- Operation with constant hydraulic motor displacement control
- Motor displacement equal to 30, 35, 65, or 80 cc/rev
- Float on down-wave side of hull (float angle < 180°) for entire 30 minute period
- Mean wave direction within 15° of device heading

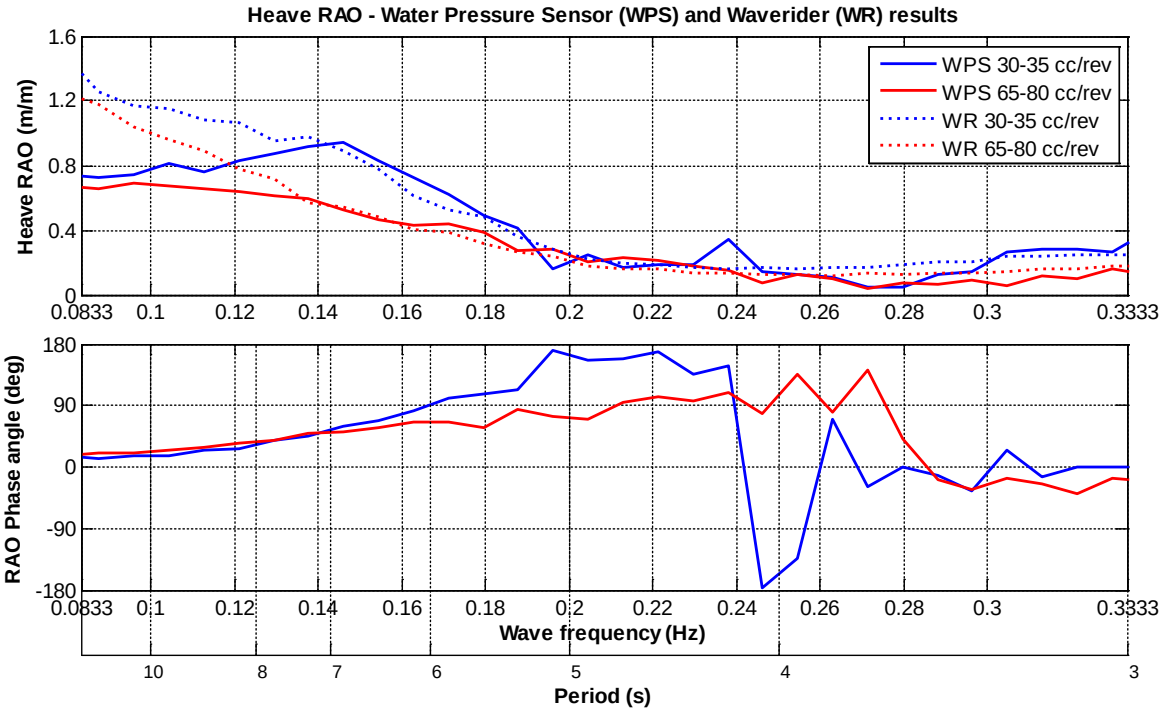


**Figure 5-18 Hull heave RAO results January-March with Te<8s and 1.6m<Hm0<2.4m**

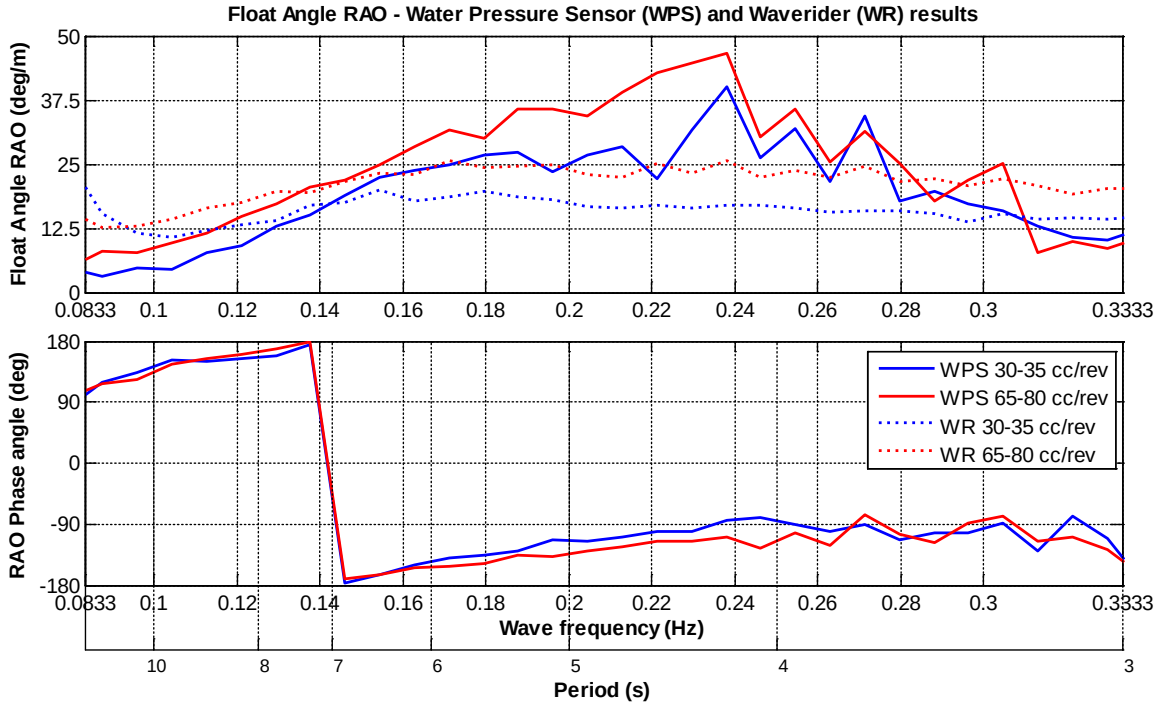


**Figure 5-19 Float angle RAO results January-March with Te<8s and 1.6m<Hm0<2.4m**

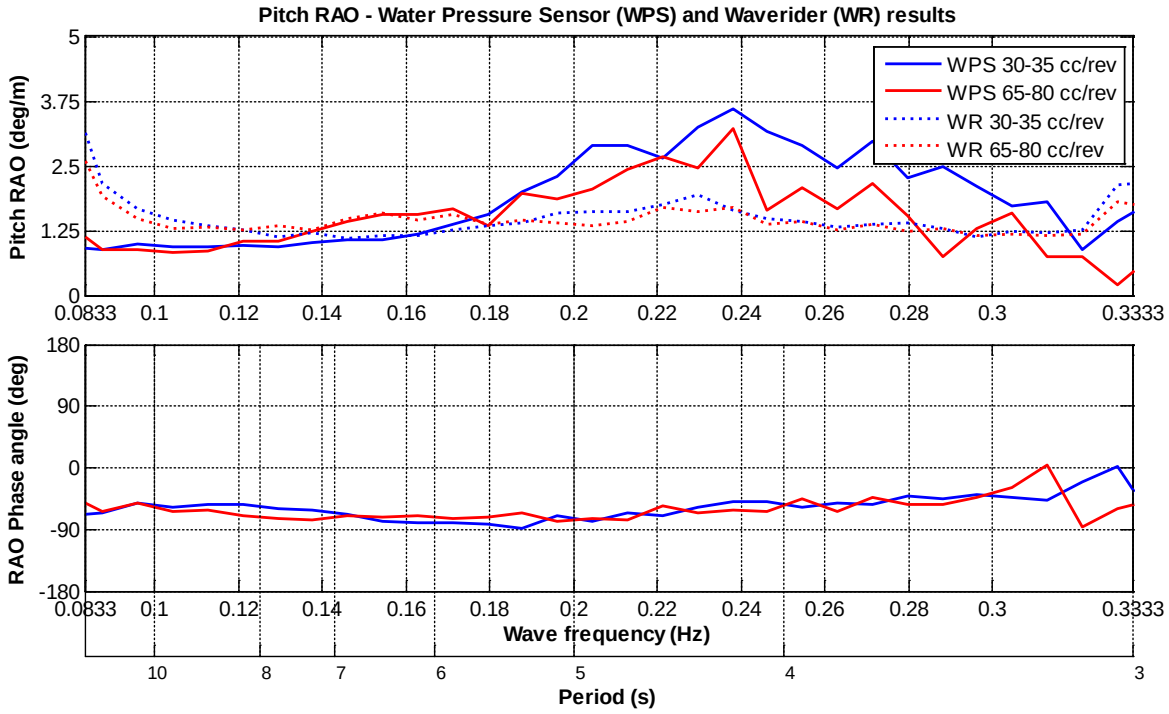


**Figure 5-20 Hull pitch RAO results January-March with Te<8s and 1.6m<Hm0<2.4m**

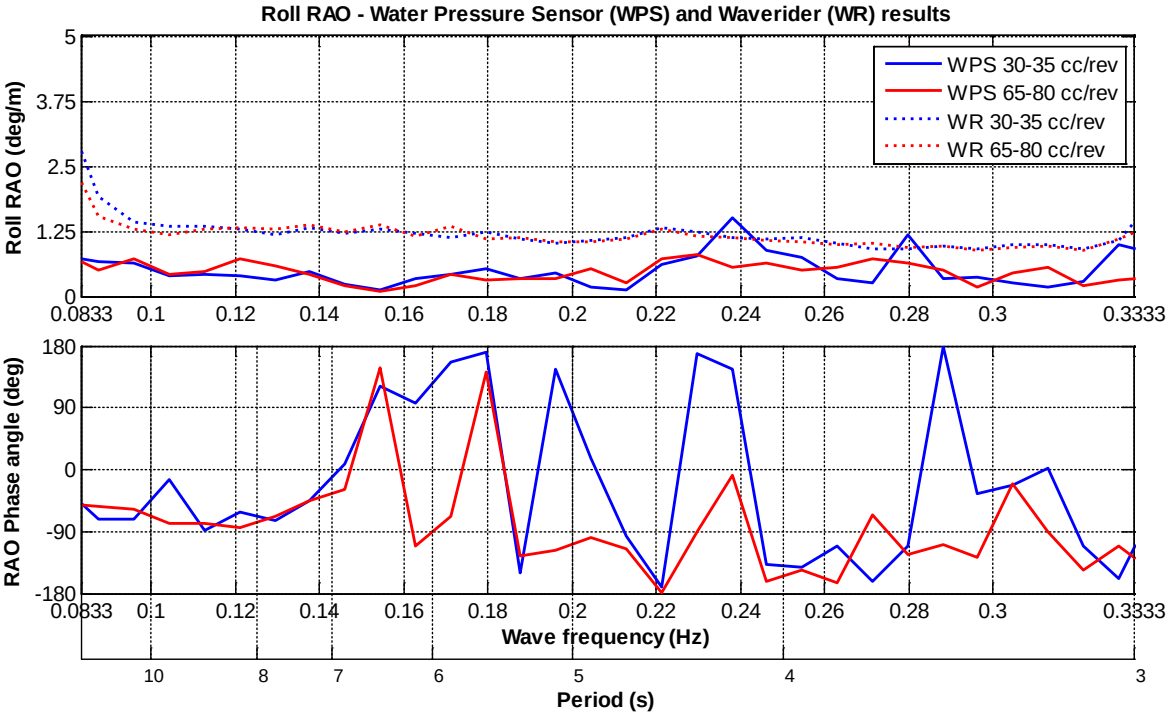


**Figure 5-21 Hull roll RAO results January-March with Te<8s and 1.6m<Hm0<2.4m**

**Table 5-3 Natural periods of prototype Azura float and hull**

| Body | Natural period | Notes |
|---|---|---|
| Float | 3 s | The uncoupled rotational natural period (pitch) of the float about its axle<br>*T*=Period (sec) $T = 2\pi\sqrt{\frac{Mk^2 + A_{pitch}}{C_{pitch}}}$<br>*M*=Mass of float (kg)<br>*k*=Radius of gyration (m)<br>$A_{pitch}$ = Added moment in pitch mode (kg m$^2$)<br>$C_{pitch}$ = Pitch restoration term (kg m$^2$/s$^2$ ; function of the distribution of water plane area and distance between center of gravity and center of buoyancy) |
| Hull | 14 s | The uncoupled heaving natural period of the hull<br>$T = 2\pi\sqrt{\frac{M + A_{heave}}{C_{heave}}}$<br>*T*=Period (sec)<br>*M*=Mass of float (kg)<br>$A_{heave}$ = Added mass of hull in heave (kg)<br>$C_{heave} = \rho g A$ (kg/s$^2$), where $\rho$ is the density, *g* is the acceleration due to gravity and *A* is the area of water plane. |
| Hull and float , coupled through PTO at axle, with viscous damping coefficients included | 6 s | Using HINMREC's WEC-Sim numerical model, cases were carried out in regular waves with constant height and varying periods. Results of power output were used to estimate the resonance period. |

*Natural period estimates made by HINMREC staff*

Several trends can be seen in the RAO results shown in Figure 5-18 through Figure 5-21:

- Hull heave noticeably increased at wave periods longer than about 6 seconds.
- The greatest float angle movement occurred at periods of 4-5 seconds; above 6 seconds there was much less float movement.
- Both the pitch and roll motions of the hull were low at all wave periods, less than 3 degrees/m and 1.5 degrees/m respectively.

The trends in hull heave and float angle movement are consistent with the natural periods of the prototype Azura float and hull. See Table 5-3 for estimates of these natural periods, provided by HINMREC. The natural period of the float is 3 s, so the greatest float angle

movements are expected at 3 s and longer periods. Movement of the float relative to the hull at longer wave periods is reduced by hull motion. The natural period of the hull alone is 14 s, however, when the device is operating the float is coupled to the hull and hull motions can be more closely estimated using the 6 s natural period of the hull and float coupled together. At wave periods longer than 6 s, the float and hull no longer act like two independent bodies and increasing hull heave motion and decreasing relative motion between the float and hull is expected. Float angle motion is therefore expected to be greatest in the 3 s to 6 s range, while hull heave motion is expected to increase at wave periods above six seconds, consistent with the hull heave and float angle RAO results shown in Figure 5-18 and Figure 5-19, respectively.

### 5.8.2 Relative capture width

PTO input power measurements made on board the prototype Azura together with time series wave elevation measurements made by the Kaneohe Bay Waverider buoy were used to calculate Relative Capture Width (RCW) of the device with respect to wave frequency. The RCW was calculated from the power and wave spectra for each 30 minute data period as follows:

$$RCW(\omega) = \frac{real\left(\frac{P(\omega)}{J(\omega)}\right)}{float\ width}$$

Where P(ω) is the PTO input power spectra of the device and J(ω) is the wave energy flux spectra. The Azura PTO input power spectra were calculated for multiple 30 minute data periods as follows:

$$P(\omega) = \frac{2\,dt^2}{T} * \text{ fft}(\text{cylinder pressure}) * \text{conj}(\text{fft}(\text{cylinder flow}))$$

Where cylinder flow and pressure are alternating hydraulic pressure and flow at the PTO input. While cylinder pressure was directly measured by pressure sensors PT01, PT02, PT07, and PT08 (see Figure 5-16 for sensor locations), cylinder flow was calculated from the rectified flow measurement using the sign of cylinder pressure. PTO input power was used because calculation of RCW with respect to wave frequency requires a power measurement that alternates with wave frequency. The calculation can't be directly done with PTO output power because the wave frequency information is lost due to PTO rectification and power smoothing.

The wave energy flux spectra were calculated as follows:

$$J(\omega) = \rho\ g\ C_g(\omega)\ S(\omega)$$

Where ρ is water density, g is acceleration of gravity, $C_g(\omega)$ are wave group velocities at frequencies of the wave spectra, and S(ω) is the wave spectra calculated by taking the FFT of time series wave elevation data recorded by the Waverider buoy.

The same January through March 2016 data set used for RAO calculations described in the preceding section were used for the RCW calculations. Like the RAO calculations, RCW was calculated separately for multiple 30 minute data periods then all results averaged to smooth the data. Data used for the RCW analysis was selected from the full January through March 2016 data set using the same method used for the RAO calculations; all 30 minute data periods with constant displacement motor control, Te<8s and 1.6m<Hm0<2.4m, and down-wave float angles were included. In the case of the RCW analysis, data with

mean wave headings of both <15° or >45° relative to device heading were processed separately for comparison. The results of this analysis are shown in Figure 5-22, together with a plot of the Kaneohe Bay annual wave flux distribution. This annual wave energy flux distribution was calculated by first averaging two years of Waverider buoy spectral data, then calculating the corresponding average wave energy flux and normalizing. This annual distribution was used to provide a comparison between the wave climate at the WETS test site and the relative capture width with respect to wave frequency or wave period of the prototype Azura.

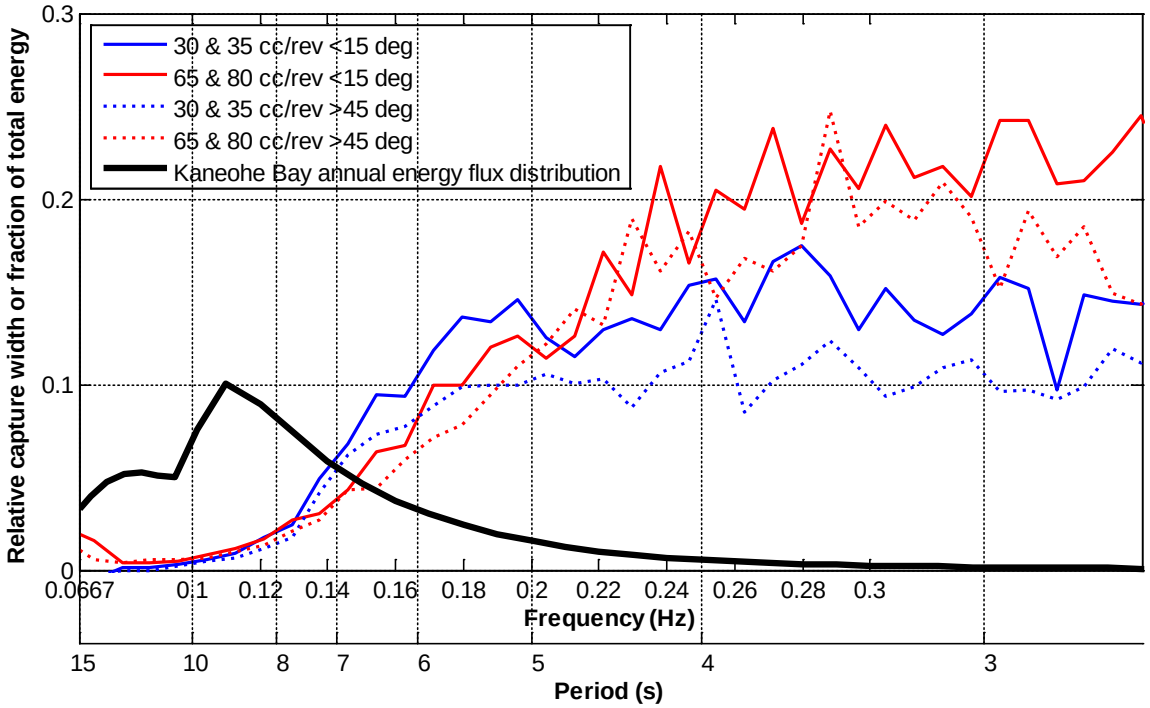


**Figure 5-22 RCW results January-March with Te<8s and 1.6m<Hm0<2.4m**

The RCW results in Figure 5-22 show that the device is most effective at producing power from waves with about 4 second periods or less, and does not produce significant power from wave periods greater than about 6-7 seconds. This is consistent with both the natural periods of the device, shown in Table 5-3, and the float angle RAO results shown in Figure 5-19, which show little float angle motion at the longer wave periods. As discussed in the previous section, at wave periods longer than the 6 s natural period of the hull coupled to the float, the float and hull no longer act like two independent bodies. Increasing hull heave motion, decreasing relative motion between the float and hull, and decreasing power production occur. Since the bulk of wave energy at the test site occurs at wave periods longer than 6-7 seconds, this poor long period response limits the energy production of the prototype device at the WETS site. This is an expected result, however, because the prototype Azura is a small-scale prototype device that, due to its short resonant periods, was not expected to be well tuned to the wave periods at WETS. A larger full scale device with longer resonant periods would be better tuned to the ocean conditions at the site.

The RCW results in Figure 5-22 also show that the device response has a small amount of directional sensitivity. More output power is produced when the mean wave heading is less than 15 degrees from device heading than when the mean wave heading is more than 45 degrees from device heading. The RCW curves are very roughly 10% higher across most of the frequency spectra when the device is lined up with the waves than when the waves approach at larger angles.

## 5.9 Time series data plots for typical device operation

Sample time series plots for typical prototype Azura operation are included in Appendix I. These plots present 10 Hz data recorded by the NWEI controller for float angle, hydraulic flow, hydraulic pressure, motor speed, and output power. Four sets of plots are included, two sets for high output power conditions with both 30 cc/rev and 80 cc/rev motor displacement, and two sets for medium output power at same the two motor displacements.

## 5.10 Other measurements

### 5.10.1 Average float angle

Thirty minute averages of data from the two prototype Azura float angle sensors are plotted in Figure 5-23 together with 30 minute average device output power for the period June 2015 through March 2016. Float angle sensor 1 is a 0-360 degree sensor that reads zero when the float is in a horizontal position on the south side of the hull (normally the down-wave or trailing side of the hull) and reads 90 degrees when the float is oriented vertically (hanging straight down). Float angle sensor 2 is a 0-180 degree sensor that reads zero when horizontal on either side of the hull and 90 degrees straight down. These 30 minute average plots show the ballasting level of the prototype Azura hull and show the time periods where the float was on the north side of the hull. The ballasting goal during the Azura deployment was to operate the device with an average float angle of zero. See Figure 5-24 for the relationship between the equilibrium hull position and average float angle. The hull equilibrium position changes by about 0.1 meters for every four degree change in average float angle. The prototype Azura hull ballast can be adjusted by adding or releasing air from the hull.

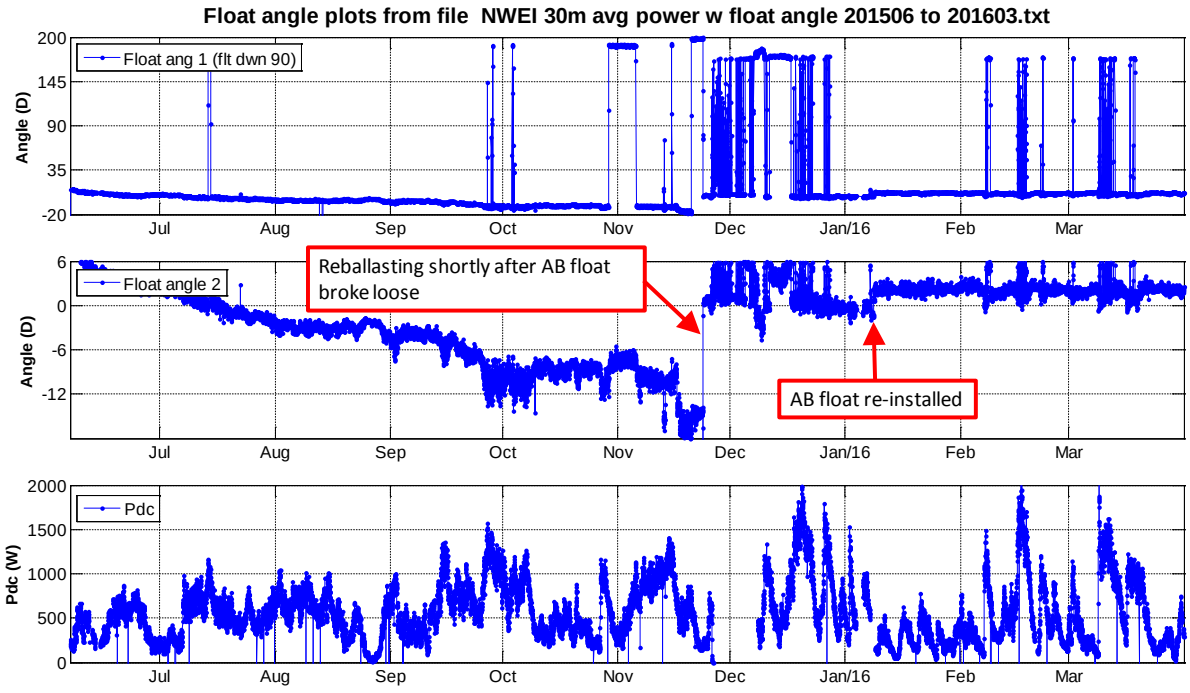


**Figure 5-23 Thirty minute average float angle plots June 2015 – March 2016**

When initially deployed at the end of May 2015, the Azura average float angle was about six degrees, indicating that the hull was ballasted about 0.15 m high. The hull slowly settled in the water over the next 5 months, until in November 2015 the average float angle was about -12 degrees, indicating that the hull was ballasted about 0.3 m low by that time. This may have been caused by the foam-filled center ballast tanks soaking up a small amount of water during this time period. In November 2015, air was added to re-ballast the hull. Since that time, the average float angle has stayed between about zero and three degrees, indicating that the hull is no longer settling in the water. A small increase in average float

angle occurred when the AB mooring float was re-installed in January 2016, due to the change in hull level caused by the presence of this float.

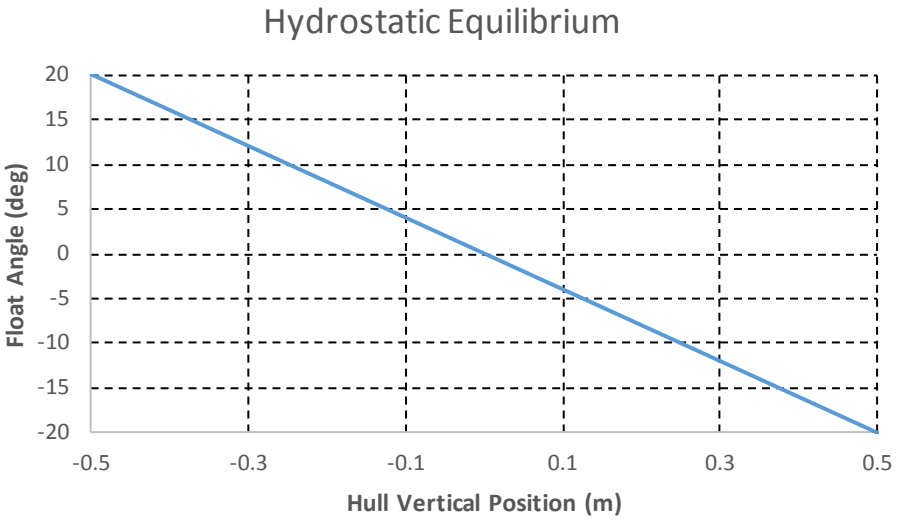


**Figure 5-24 Relationship between hull and float equilibrium conditions**

The 30 minute average float angle 1 data also shows when the float has moved from one side of the hull to the other. The device was deployed in May 2015 with the float on the south side of the hull, which is indicated by a -90 to 90 degree average float angle. Since then, during numerous short time periods while the device has been producing higher power, the float has flipped to the north or up-wave side of the hull. In extremely energetic seas, indicated by high output power, the float repeatedly has flipped from one side of the hull to the other. Since the prototype Azura is designed for the float to rotate 360 degrees and the PTO operates equally well with the float to either side of the hull, float rotation does not affect performance or survivability of the device.

### 5.10.2 Temperatures

Temperature measurements were logged for a few components and enclosures on board the device by the NWEI cRIO controller and also a WebRelay temperature and humidity sensor. The maximum temperatures that were recorded by these sensors throughout the deployment period are shown in Table 5-4. Also included in Table 5-4 are air temperature, water temperature, and wind speed measurements made at these times by the National Data Buoy Center (NDBC) station at Mokuoloe, HI, about 3 miles from the test site.

None of the maximum temperatures recorded were above the expected temperature ranges for these components or enclosures. The cRIO controller is the NWEI controller that records data and controls the PTO. This controller is rated for operation in ambient temperatures as high as 70 °C with the controller chassis itself capable of much higher temperatures. The maximum recorded temperature of ambient air inside the cRIO enclosure was 40 °C and the corresponding maximum chassis temperature was 56 °C, well within the device ratings. The interior temperature of the device drybox, which houses the instrumentation power supply for the device, did not exceed 32 °C which was approximately equal to the temperature of the surrounding air and sea water when the measurement was made. The maximum controller and drybox temperatures occurred when output power of the device was relatively

low but outside air and water temperatures were high; heat losses by other components in the PowerPod did not significantly affect these temperatures. The maximum generator and transformer winding temperatures of 76 °C and 65 °C, however, did occur during a period with high device output power. These devices are both built with windings that are rated to at least 180 °C, so these temperatures are well within the capability of these components.

**Table 5-4 Maximum temperature measurements June 2015 – March 2016**

| | Maximum Temp (°C) | Date Time (UTC) | Air Temp °C | Water Temp °C | Wind Speed (m/s) | Output Power (W) |
|---|---|---|---|---|---|---|
| **cRIO controller chassis** | 56 | 9/2/2015 10:40 | 33 | 30 | 1 | 410 |
| **cRIO controller enclosure*** | 43 | 9/3/2015 1:00 | 30 | 30 | 3 | 425 |
| **Drybox*** | 32 | 9/11/2015 1:00 | 33 | 30 | 3 | 150 |
| **Generator windings** | 76 | 12/20/2015 11:30 | 24 | 24 | 11 | 1958 |
| **Transformer windings** | 65 | 12/20/2015 11:30 | 24 | 24 | 11 | 1958 |

* Temperatures only recorded once per day by WebRelay X-300 at 1:00 UTC

### 5.10.3 Drybox and NWEI cRIO controller enclosure humidity

The humidity of both the drybox and the NWEI cRIO controller enclosure on board the device are plotted for the entire June 2015 through March 2016 deployment period in Figure 5-25. These measurements were logged by WebRelay X-300 humidity sensors installed inside these enclosures. The cRIO controller enclosure is located inside the main cavity of the PowerPod, while the drybox is a welded protrusion on the PowerPod that is sealed from the rest of the PowerPod cavity. Sensitive electronics are housed inside each enclosure so low humidity is important. Prior to the prototype Azura deployment, desiccant was placed inside both enclosures and the inside of the PowerPod was also purged with nitrogen. The humidity measurements in Figure 5-25 indicate that both enclosures maintained much lower humidity than outside air, however, the drybox maintained lower humidity than the controller enclosure. Most likely this is because the drybox is well sealed from the remainder of the PowerPod cavity, while the controller enclosure does not have air-tight sealing from surrounding air inside the PowerPod.

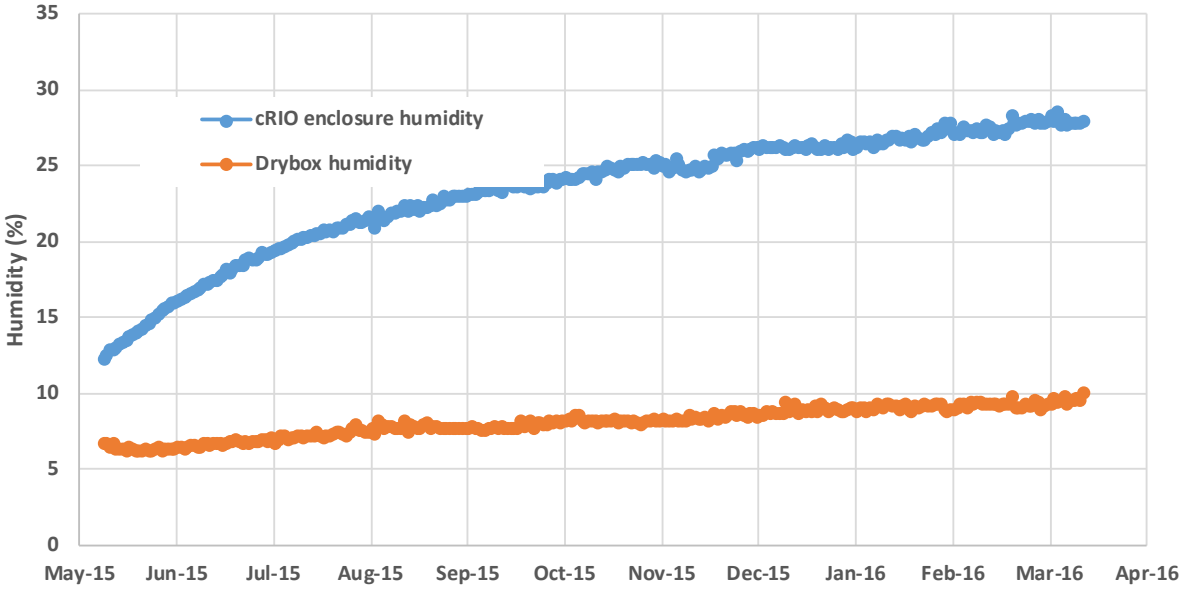


**Figure 5-25 cRIO and drybox enclosure humidity measurements June 2015 – March 2016**

# 6. Conclusions

These tests successfully demonstrated ten months of reliable prototype Azura operation at the WETS 30 m site. Specific conclusions that can be drawn from the results are as follows:

- The device survived sea conditions with $H_{m0}$ as high as 4.5 m and individual waves as high as 7.5 m during the test period
- High availability was demonstrated for the device during the test period, with over 98% availability during several months. The device was capable of operation throughout the ten month period, with the exception of one 12 day period after a hydraulic hose became loose.
- Power performance of the device was measured with constant motor displacement operation. The results show 30 minute normalized power as high as 2240 W. Output power always increased with decreasing $T_e$ for the same $H_{m0}$, with the highest power for a given $H_{m0}$ always occurring in the minimum $T_e$ bins.
- While the full range of PTO hydraulic motor displacement settings were tested over a long period of time, the results show that motor displacement only had a small effect on device output power.
- Output power of the device was not substantially higher when PI control of PTO hydraulic motor displacement was used than when constant motor displacements were used.
- PTO efficiency was approximately 65% to 70% at higher (greater than 1500 W) output power.
- RAO results show that hull motion noticeably increased at wave periods longer than about 6 s, and the greatest float angle movement occurred at 4 s to 5 s wave periods. These results are consistent with the natural periods of the hull and float; increased hull motion is expected at periods longer than the coupled hull-float resonant period of 6 s, and the greatest float motion is expected at periods between the float resonant period of 3 s and the coupled hull-float resonant period of 6 s. The RAO results also show that there is very low pitch and roll motion of the hull across the full range of wave periods.
- RCW results show that the prototype device is most effective at producing power from wave periods of four seconds or less in the spectra, and does not produce significant power for wave periods longer than six or seven seconds. This is consistent with the natural periods of the device; the greatest power production is expected at longer periods than the float natural period (3 s) and shorter periods than the coupled hull-float natural period (6 s). Since the bulk of the wave energy at the test site occurs at wave periods longer than six or seven seconds, this poor long period response greatly limited power production for this prototype at the WETS site. This is an expected result, however, because the prototype Azura is a small-scale prototype device that, due to its short resonant periods, was not expected to be well tuned to the wave periods at WETS. A larger full scale device with longer resonant periods would be better tuned to the ocean conditions at the site.

# Appendix I

## Sample Time Series Plots for Typical Operation

February 17, 2016 at 5:30
Average output power = 1850 W, Motor Displacement = 30 cc/rev
Hm0 = 3.4 m, Te = 7.6 s

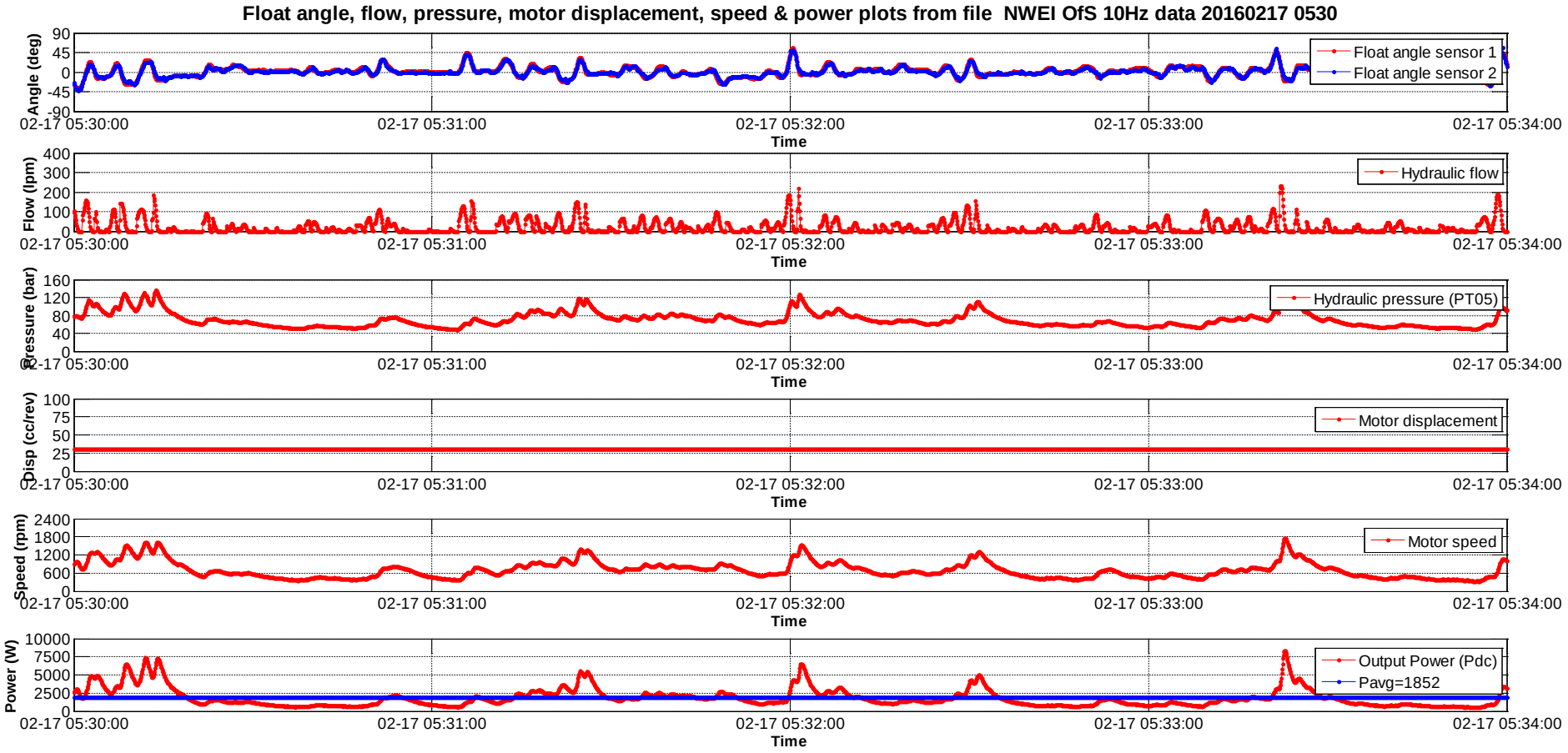

February 17, 2016 at 8:30
Average output power = 1660 W, Motor Displacement = 80 cc/rev
Hm0 = 3.6 m, Te = 7.9 s

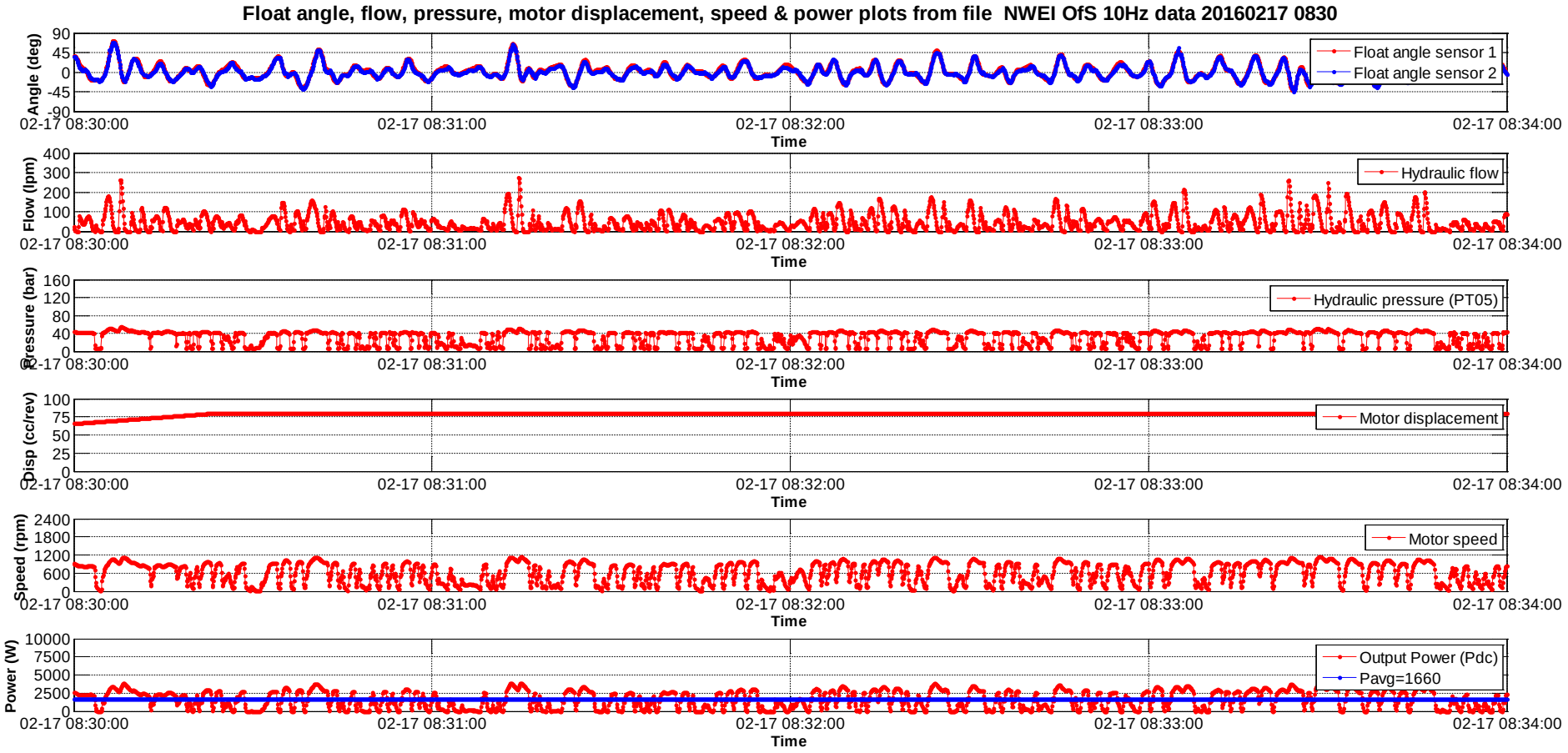

February 26, 2016 at 12:00
Average output power = 540 W, Motor Displacement = 30 cc/rev
Hm0 = 3.0 m, Te = 12.5 s

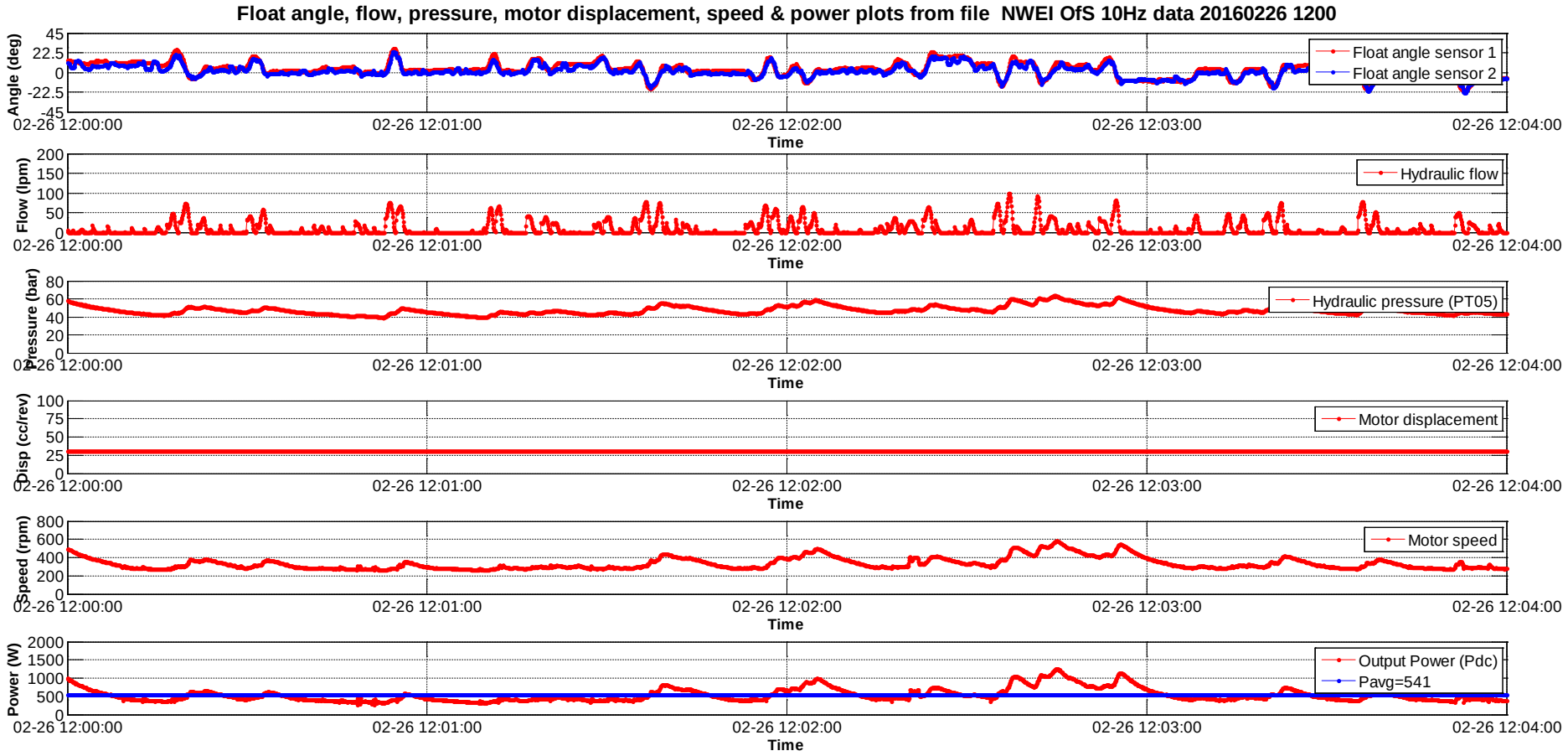

February 26, 2016 at 8:30
Average output power = 560 W, Motor Displacement = 80 cc/rev
Hm0 = 3.1 m, Te = 13.0 s